

# Dominant trends in Jupiter's H+3 northern aurora: II. magnetospheric mapping

Article

Published Version

Creative Commons: Attribution 4.0 (CC-BY)

Open Access

Stallard, T. S. ORCID: https://orcid.org/0000-0003-3990-670X, Knowles, K. L. ORCID: https://orcid.org/0000-0001-5055-8115, Melin, H. ORCID: https://orcid.org/0000-0001-5971-2633, Wang, R. ORCID: https://orcid.org/0000-0002-4563-8919, Thomas, E. M. ORCID: https://orcid.org/0000-0002-5773-6110, Moore, L. ORCID: https://orcid.org/0000-0003-4481-9862, O'Donoghue, J. ORCID: https://orcid.org/0000-0002-4218-1191, Johnson, R. E. ORCID: https://orcid.org/0000-0002-4218-1191, Johnson, R. E. ORCID: https://orcid.org/0000-0002-0166-6854 (2025) Dominant trends in Jupiter's H+3 northern aurora: II. magnetospheric mapping. Journal of Geophysical Research: Space Physics, 130 (10). e2025JA034076. ISSN 2169-9402 doi: 10.1029/2025ja034076 Available at https://centaur.reading.ac.uk/125096/

It is advisable to refer to the publisher's version if you intend to cite from the work. See <u>Guidance on citing</u>.

To link to this article DOI: http://dx.doi.org/10.1029/2025ja034076

Publisher: American Geophysical Union (AGU)



All outputs in CentAUR are protected by Intellectual Property Rights law, including copyright law. Copyright and IPR is retained by the creators or other copyright holders. Terms and conditions for use of this material are defined in the <a href="End User Agreement">End User Agreement</a>.

## www.reading.ac.uk/centaur

#### **CentAUR**

Central Archive at the University of Reading

Reading's research outputs online



## **JGR** Space Physics

### <del>-</del>

#### RESEARCH ARTICLE

10.1029/2025JA034076

#### **Key Points:**

- Jupiter's main auroral emission is statistically 3 times brighter in the region mapping to magnetospheric dusk than dawn
- Jupiter's main auroral emission statistically darkens on the magnetospheric noon-to-dawn side, and is especially dim close to noon
- Jupiter's polar auroral emission morphology varies significantly with local time, only sometimes matching in structure to polar models

#### **Supporting Information:**

Supporting Information may be found in the online version of this article.

#### Correspondence to:

T. S. Stallard, tom.stallard@northumbria.ac.uk

#### Citation:

Stallard, T. S., Knowles, K. L., Melin, H., Wang, R., Thomas, E. M., Moore, L., et al. (2025). Dominant trends in Jupiter's H<sub>3</sub><sup>+</sup> northern aurora: II. magnetospheric mapping. *Journal of Geophysical Research: Space Physics, 130*, e2025JA034076. https://doi.org/10.1029/2025JA034076

Received 11 APR 2025 Accepted 4 SEP 2025

#### **Author Contributions:**

Conceptualization: Tom S. Stallard

Data curation: Tom S. Stallard
Formal analysis: Tom S. Stallard
Funding acquisition: Tom S. Stallard
Investigation: Tom S. Stallard
Methodology: Tom S. Stallard
Project administration: Tom S. Stallard
Resources: Tom S. Stallard
Software: Tom S. Stallard
Validation: Tom S. Stallard
Visualization: Tom S. Stallard
Writing – original draft: Tom S. Stallard
Writing – review & editing: Tom
S. Stallard, Katie L. Knowles,
Henrik Melin, Ruoyan Wang, Emma
M. Thomas, Luke Moore.

©2025. The Author(s). This is an open access article under the terms of the Creative Commons Attribution License, which permits use, distribution and reproduction in any medium, provided the original work is properly cited.

## Dominant Trends in Jupiter's H<sub>3</sub><sup>+</sup> Northern Aurora: II. Magnetospheric Mapping

Tom S. Stallard<sup>1</sup>, Katie L. Knowles<sup>1</sup>, Henrik Melin<sup>1</sup>, Ruoyan Wang<sup>2</sup>, Emma M. Thomas<sup>1</sup>, Luke Moore<sup>3</sup>, James O'Donoghue<sup>4</sup>, Rosie E. Johnson<sup>5</sup>, Steve Miller<sup>6</sup>, and John C. Coxon<sup>1</sup>

<sup>1</sup>Department of Mathematics, Physics and Electrical Engineering, Northumbria University, Newcastle upon Tyne, UK, <sup>2</sup>School of Physics and Astronomy, University of Leicester, Leicester, UK, <sup>3</sup>Center for Space Physics, Boston University, Boston, MA, USA, <sup>4</sup>University of Reading, Reading, UK, <sup>5</sup>University of Aberystwyth, Aberystwyth, UK, <sup>6</sup>Department of Physics and Astronomy, University College London, London, UK

**Abstract** Jupiter's auroral regions have previously been defined by broad-scale auroral structures, but these are typically obscured by the wide array of temporal variability observed at timescales between minutes and days, making it difficult to understand the underlying magnetospheric biases driving these brightness differences. Here, we follow on from an initial study of Jupiter's aurora, again utilizing a data set of >13,000 H<sub>3</sub><sup>+</sup> images of Jupiter mapped into latitude, longitude and local time, smoothed over tens of hours of integration and many days of observing. Having removed correlations between brightness and both magnetic field and planetary local time identified in the first study, we examine morphological changes in emission with both planetary and magnetic local time. We reveal that the H<sub>3</sub><sup>+</sup> main auroral emission is enhanced by a factor of three in the region mapping into the dusk magnetosphere. An additional strong auroral darkening is observed near noon, aligned with previous ultraviolet observations of an auroral discontinuity in this region, though this rotates duskward slightly in magnetic local time, as the ionospheric source mapping to this region moves duskward. The polar aurora contrasts with this strongly, showing brightness enhancement when the auroral pole points toward the dawn and dusk limbs. It also shows that the Dark region is fixed in local time, close to the dawnward edge of the polar region, while the Swirl region appears to match well with predictions from recent MHD models when the magnetic pole points toward dawn, but changes significantly at other magnetic pole directions.

Plain Language Summary Jupiter's aurora are complex and highly variable, making it difficult to build an understanding of the underlying processes that produce these bright 'northern lights'. Here, we combined more than 13,000 images to measure how the auroral emission changes with the changing direction of the Sun relative to the planet. In the polar regions of the planet, the shape and structure of the aurora changes significantly as the planet rotates relative to the Sun, only sometimes matching with past models of this interaction. The brightest auroral emissions are linked to the surrounding space environment in complex ways, because the solar wind bends Jupiter's magnetic fields away from the Sun farther from the planet. Accounting for this bending, we map out these bright auroral emissions, revealing the location of the drivers of Jupiter's aurora. Auroral regions mapping to the dusk side of the magnetosphere are three times brighter than the dawn, and regions mapping close to the region facing the Sun are significantly weaker.

#### 1. Introduction

Our understanding of Jupiter's bright and complex aurora is highly constrained by both the wide array of auroral morphologies observed from one day to the next, the diverse potential sources for these auroral emissions and difficulty in modeling these complex systems. However, some aspects of Jupiter's aurora morphology are so dominant that they are apparent within every individual night of observation. Although the aurora of Jupiter are contiguous, with numerous individually named features, the complex and interacting auroral emissions are traditionally split into three groups: those originating equatorward of the main emission, the main auroral emission itself and the polar aurorae (Grodent, 2015).

In Figure 1, for context, we highlight the different auroral regions as they appear both Juno-JIRAM and IRTF-NSFCAM images. Notably, these two views are taken from very different perspectives, JIRAM views the aurora from the dawnward direction at incredible spatial resolution (though, for JIRAM, this is an anomalously low-resolution image, with most JIRAM images being taken directly over the polar region, much closer to the

STALLARD ET AL. 1 of 24

from https://agupubs.onlinelibrary.wiley.com/doi/10.1029/2025JA034076 by NICE, National Institute for Health and Care Excellence, Wiley Online Library on [16/10/2025]. See the Term

James O'Donoghue, Rosie E. Johnson, Steve Miller, John C. Coxon

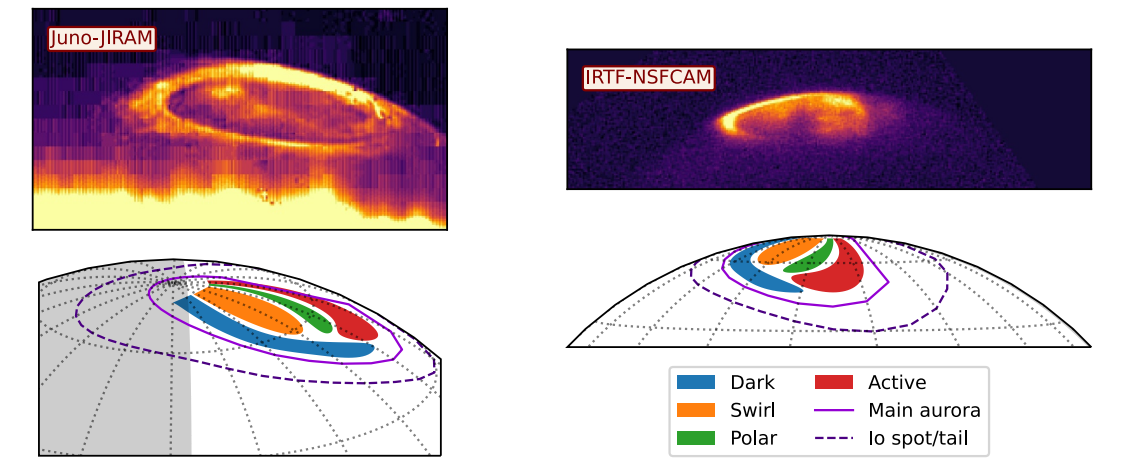


Figure 1. Example images of Jupiter's aurora from JWST and IRTF. Each image (top) shows a single raw frame (with a sky subtraction for IRTF), highlighting the contrasting views seen from each telescope. Both telescopes utilize a very narrow near-infrared wavelength  $H_3^+$  filter, allowing emission from the ionosphere to be observed above the significant absorption of methane at similar wavelengths. Each images is independently normalized to the brightest auroral features. The JIRAM image is a 1 s integration taken on 26 August 2016 at 16:32 UT, the day before PJ1 perijove. The image was taken at a solar phase angle of 92.4°, so that only the right hand side of the image is sunlit, and at sub-Juno longitude of 271°W. The L-band imager covers 3.32–3.60  $\mu$ m (a spectral resolution of R  $\approx$  12) The IRTF-NIRSPEC image is a 5 s integration taken on 27 August 1998 at 11:38 UT. The image was taken using a 3.4265  $\mu$ m filter (R  $\approx$  200) at a sub-Earth longitude of 171°W. The solar phase angle of 5°, so small, the entire disk is effectively sunlit. Below these are are representation of the different auroral features see from the viewing angle of these images, with the locations of the main auroral emission and Io spot and tail taken from Grodent et al. (2008) and an estimation of the four polar regions based upon the regions outlined in Stallard et al. (2016), in turn originally based upon (Grodent, Clarke, Waite, et al., 2003). Sunlit parts of the disk are shown in white, contrasted with nightside in gray.

planet). However, image quality is somewhat impaired by the relatively low spectral resolution (R  $\approx$  12), light bleeding from the much brighter M-band filter (causing the bright [patterns] streaking in from the bottom of the image), vertical striations from instrument effects, as well as compression effects in the data and significant noise from Jupiter's radiation environment. In contrast, IRTF-NSFCAM images the planet from Earth, with the sun almost directly behind us. Having a large and stable instrument that can be maintained by expert in-house engineers results in much less noisy data, aided further by the much higher spectral resolution (R  $\approx$  200) reducing background emission from Jupiter. However observing from Earth results in turbulence within the skies above Mauna Kea, significantly smoothing out the auroral images from Jupiter, and observations are fixed in solar local time, with all observations occurring when the central meridian is close to noon.

However, both images reveal clear structures in the emissions from the molecular ion  $H_3^+$ , both across the planetary disk, generated by solar EUV ionization., and more dramatically within the auroral region, generated by particle precipitation. Here, we outline our current understanding of these different forms of auroral emission:

#### 1.1. Equatorward Auroral Emissions

The most equatorward auroral emission observed at Jupiter are those that map along magnetic field to the volcanic moon Io, generating both a series of bright spots at its footprint and an extended tail (Bonfond et al., 2017; Connerney et al., 1993; Mura et al., 2018), with the multiple (and often complex) spots generated as a result of Alfvén wave interactions from the moon itself. The other Galilean moons also produce similar auroral signatures although, because these moons are further from the planet, the resultant spots fall close to or inside the main emission (Hue et al., 2023).

Between Io's magnetic footprint and the main auroral emission, a broad arc of diffuse "equatorial" emission exists, also known as a "secondary" auroral oval, enhanced in both brightness and longitudinal spread 1–3 days after large magnetospheric hot plasma injections (Gray et al., 2017). This diffuse emission is typically associated with whistler-mode waves driving energetic electron scattering (Gray et al., 2017; Radioti et al., 2009), but sometimes includes very bright localized emission features, associated with plasma injections from the

STALLARD ET AL. 2 of 24

magnetotail (Grodent, 2015) or with plasma produced from volcanic material from Io (Bonfond et al., 2012). Juno observations of energetic particles in the space immediately above this region have confirmed that this diffuse emission is driven by wave-particle scattering driving particles into the atmosphere. The electrons from wave-particle scattering (within the upward loss cone) then present lower intensities and energy fluxes due to removal by the atmosphere (Mauk et al., 2020).

#### 1.2. Main Auroral Emissions

Following detailed in situ measurements by the Juno spacecraft, we now understand Jupiter's main auroral emission to be a complex blend of auroral morphologies and magnetospheric drivers. The aurorae of Jupiter have been observed over a wide range of wavelengths, including prompt ultraviolet (UV) emission from upper atmospheric H and  $H_2$  excited by auroral participle precipitation, and thermally excited infrared emission from the  $H_3^+$ , ionized by auroral particle precipitation. The two dominant components of these emissions within the main auroral region appear to be:

- 1. A relatively narrow bright arc; this arc, which is relatively UV bright, undergoes significant hydrocarbon absorption in the UV, suggesting it originates from deep below the homopause. Driven by deeply penetrating precipitation (Gérard et al., 2018) associated with predominantly upward currents (also named Zone-I aurora; Mauk et al., 2020), this suggests they are aligned with the steady-state auroral current system driven by plasma flows in the magnetosphere that was traditionally seen as the main driver of Jupiter's auroral emission (Hill, 1979). However, there remains some controversy around how these emissions are driven. Notably:
  - Mauk et al. (2017) used Juno data to show that Jupiter's auroral downward energy flux from discrete
    acceleration is less than that caused by broadband or stochastic processes, and Salveter et al. (2022) found
    that the originating isolated mono-energetic electron distributions make up only 7% of the final precipitating electron population.
  - However, J. D. Nichols and Cowley (2022) found a clear statistical relationship between the peak auroral
    UV intensity, measured by HST, and longitudinally co-located magnetospheric radial current, measured by
    Juno. This revealed that changing breakdown-in-corotation current strength is a direct driver of changing
    auroral brightness, at least on the dawn side of the planet.
  - Seemingly in direct conflict, one solution to this is suggested by Zhang et al. (2021), that that coherent
    discrete acceleration might trigger instabilities, broadening electron distributions through stochastic processes. So there might exist an approximately linear relationship between the breakdown-in-corotation
    current strength and in the instabilities that cause the precipitation that actually power the aurora.
- 2. A broader region of multiple scattered arcs, relatively bright within the H<sub>3</sub><sup>+</sup> infrared emission compared with the UV (Gérard et al., 2018). These are associated with broadband flux precipitation that is highly bidirectional, with a bias toward downward currents (Mauk et al., 2020), and has been associated with pitchangle scattering processes, since the aurora within this downward current region might be expected to have even stronger aurora where the upward currents close into the magnetosphere (since upward currents would accelerate electrons into the atmosphere), but the matching upward current regions are markedly absent of any auroral emissions (R. Wang et al., 2023). However, Juno's Jupiter Energetic Particle Detector Instrument (JEDI) has identified very high energy (>10 MeV, perhaps >100 MeV) upward electron beams accelerated from the planet. How auroral processes accelerate such beams out from Jupiter is unknown (Mauk et al., 2024).

Since these two dominant forms of aurora are broadly co-located, separating them morphologically is very tricky. However, taken collectively, the overall structure and brightness is most strongly affected by the magnetic field mapping from the ionosphere out into the surrounding magnetosphere (Kivelson & Southwood, 2005). This is most evident in the broad scale shape of the northern and southern auroral regions. In the north, the distorted magnetic field results in the main emission following an approximately circular morphology on the western side and a highly kinked shape on the eastern side (Connerney et al., 2022; Grodent et al., 2008), while in the south, the aurora sits closer to the pole and is a more circularized oval morphology (Connerney et al., 2022), as shown later in Figure 2.

The detailed morphology of these aurorae is confused by local time changes. Observations from Earth have long shown the main auroral emission appearing narrow at dawn and fragmented at dusk (Gerard et al., 1993; Grodent, Clarke, Kim, et al., 2003). While recent Juno observations have partially confirmed this is a local time effect (Gérard et al., 2018), the auroral oval appears highly fragmented across all local times (Mura et al., 2017; see

STALLARD ET AL. 3 of 24

ntlinelbtary.wiley.com/doi/10.1029/2025/A034076 by NICE, National Institute for Health and Care Excellence, Wiley Online Library on [16/10/2025]. See the Terms and Conditions (https://onlinelibrary.wiley.com/term

conditions) on Wiley Online Library for rules

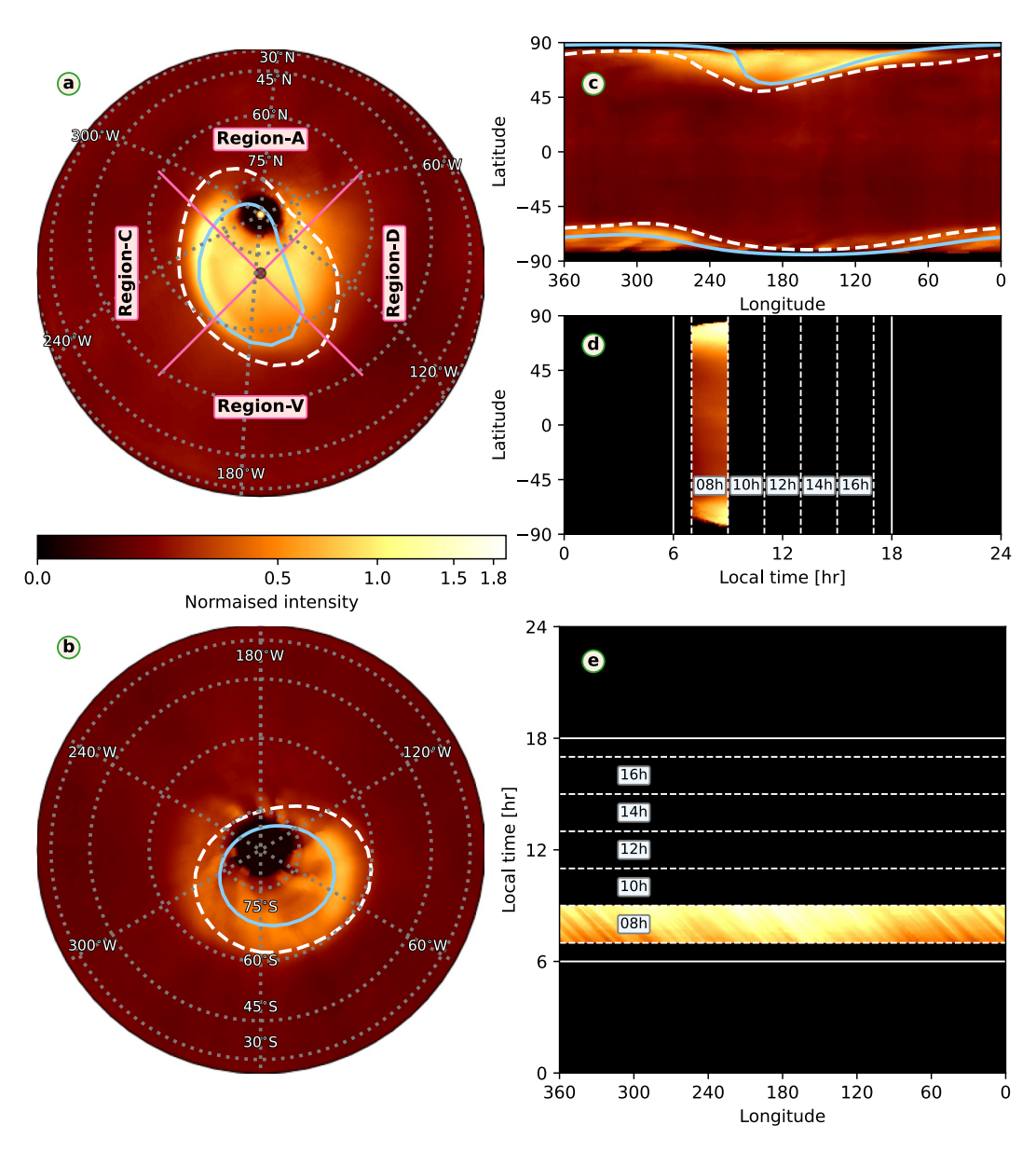


**Figure 2.** Maps of average emission, normalized the mean auroral brightness, across the three dimensions. The average intensity summed across planetary local times between only 07:00 and 09:00 is shown in both polar projection (north and south) in panel (a) and (b) respectively, and in cylindrical projection in panel (c). The average intensity summed across all longitudes is shown in panel (d). The average intensity summed across all latitudes is shown in panel (e). All maps are shown with a gamma stretch of 0.5, with a maximum value that best shows the overall emission structure. Panels (a–c) show the location, modeled statistical location of the ultraviolet main emission (solid blue) and Io spot (dashed white), taken from Grodent et al. (2008). Panels (d) and (e) show five groupings of local time, each 2 hr wide, centered on 08, 10, 12, 14, and 16 hr.

Figure 1), with the extent of this fragmentation appearing to change across the entire oval with time, rather than just at dusk (Greathouse et al., 2021). One notable difference between UV H and  $H_2$  emission and infrared  $H_3^+$  emission, seen clearly in those observations where both wavelengths are observed at the same time, is that at least the dusk side is notably more fragmented in the  $H_3^+$  emission (Gérard et al., 2018). At high resolution, the  $H_3^+$  main emission has no clear main oval but instead consists of roughly 10 separate arcs of emission of approximately similar brightness (Mura et al., 2017). In the UV, a matching broader region of emission is seen, but is often significantly weaker than a single arc of main emission that appears to have significant hydrocarbon absorption in comparison to the surrounding regions (Gustin et al., 2016).

STALLARD ET AL. 4 of 24

Statistical analysis of the UV main emission brightness has shown that the dusk side is a factor of 3 times brighter than the dawn in the south, but only 1.1 brighter in the north (Bonfond et al., 2015). Since the southern aurora sees significantly less magnetic field strength differences than the north, Bonfond et al. (2015) suggest once magnetic field differences are accounted for, both hemispheres should appear more like the south, with the strong dusk enhancement driven by a different significant source. The main oval also dims significantly near noon (Caldwell et al., 1992), a discontinuity that is present in both hemispheres and confined in magnetospheric local time in the prenoon and early noon sector (Radioti et al., 2008), suggesting a magnetospheric origin for the brightness change.

Rutala et al. (2024) presented the first large-scale statistical survey of Jovian mean UV auroral emission, finding large variability in brightnesses peaking at mapped distances between 20 and 30  $R_J$ . However, this mapping did not account for either surface magnetic field or the changing affects of solar-ionization with planetary local time, which are both modeled to have strong affects on the auroral emission strength (Ray et al., 2014; Tao et al., 2010 respectively), and, as we will describe below, were both shown to have a dominant effect on  $H_3^+$  emission strength in the companion to this paper. Notably, Rutala et al. (2024) does not show a clear anti-correlation between magnetic field strength and UV brightness, with no apparent longitudinal changes in brightness, and northern UV brightnesses typically brighter than in the south. This hemispheric difference is in direct contrast with both past UV measurements (Bonfond et al., 2015) and in situ Juno measurements in the two hemispheres Kotsiaros et al. (2019), both of which suggest the southern auroral strength (where the magnetic field is significantly weaker) is significantly higher than the north.

Chané et al. (2013) modeled the auroral differences driven by asymmetrical magnetospheric flows. These modeled flows, which are comparable to plasma flows measurements made by Galileo (Krupp et al., 2001), and more recently by Juno (e.g., J.-Z. Wang et al., 2024), modulate the breakdown in co-rotation auroral currents. This results in reduced currents in the noon-dawn sector, as plasma in that region moves much closer to the rotation rate of the planet, while in the dusk-midnight sector, plasma sub-corotates very significantly, enhancing the main auroral emission. This results in much weaker emission in ionospheric dawn-noon region, which appears to broadly match with the localized discontinuity seen by Radioti et al. (2008).

In conclusion, there are likely to be significant drivers of changing auroral emission strength between dawn and dusk, potentially consisting of both planetary local time difference within the ionosphere itself and those driven by local time differences within the magnetosphere, shaped by magnetospheric morphology and dynamics. However, decoupling these two sources of local time difference from each other and from changing magnetic field strength is not possible with past data sets.

#### 1.3. Polar Emissions

Jupiter's polar auroral region has long been confusing, with  $H_3^+$  emission previously described as having a Yin-Yang morphology (Satoh & Connerney, 1999) and UV emissions as a series of arcs of emission mapping out different magnetically mapped regions (Pallier & Prangé, 2001). However, the broad consensus now describes the northern dayside polar aurora as being split into three sub-regions, originally defined by Grodent, Clarke, Waite, et al. (2003): the Active, Dark, and Swirl regions, along with a fourth polar  $H_3^+$  emission darkening not seen in the UV (Stallard et al., 2016):

#### 1.3.1. Dark Region

Immediately poleward of the dawnside main emission, there is the narrow Dark region (blue in Figure 1), a crescent shaped region containing relatively little aurora (Grodent, Clarke, Waite, et al., 2003). Juno UV Spectrograph (UVS) identifies that this typically appears to occur within magnetic local times of 0-11 UT (Greathouse et al., 2021). In the infrared,  $H_3^+$  ion wind velocities within this region are stagnant in the observers' frame, relating these winds to the direct or indirect influence of the solar wind (Johnson et al., 2017). More recent measurements of both ion and neutral winds suggest this flows are highly coupled in this region, making it difficult to understand whether ions or neutrals are the primary driver of ionospheric flow in this region (R. Wang et al., 2023).

Recent observations by the Juno spacecraft have identified a clear mid-latitude region of the magnetosphere that Juno JEDI clearly identifies as having a solar wind  $He^{n+}/H^+$  composition (Delamere et al., 2024). Further, magnetic modeling suggests this open-field region maps into the most dawnward side of the polar cap (Zhang

STALLARD ET AL. 5 of 24

et al., 2021), identifying the open-field-line region with the Dark region. The JADE's ion instrument showed this same region significantly sub-corotates, aligning these flows with Johnson et al. (2017)'s ionospheric flows, perhaps strengthening the view this open-field-line region is Jupiter's Dark Region.

#### 1.3.2. Active Region

Poleward of the main emission on the dusk side, and toward noon, is an "Active region" of emission (red in Figure 1) that varies significantly in brightness (Grodent, Clarke, Waite, et al., 2003; Stallard et al., 2016; J. D. Nichols et al., 2025). It often includes both bright arcs of emission and localized bright spots, which are difficult to disentangle, in exact shape and position, from the Zone-II main auroral emissions, either within imaging or using in situ measurements from Juno's waves and particles instruments (Sulaiman et al., 2022). This region also produces bright hard X-ray emission from precipitating Sulfur, Carbon and Oxygen lines, with these emissions brightening during both magnetospheric compressions and expansions (Dunn et al., 2020).

These localized spots are very bright in the UV, and have been observed simultaneously within multiple Juno instruments (Haewsantati et al., 2023), including JEDI, the Jovian Auroral Distributions Experiment (JADE), the Waves instrument (Waves) and the magnetometer (MAG). That investigation showed that they originate close to the planet, since they are fixed in planetary longitude, are associated with deep UV emissions (with high color ratios), yet are dominated by upward electrons coming out of the planet. However, significant magnetic field perturbations only appear to occur for some spots, suggesting that field-aligned currents may not always be the primary driver for these auroral features. Most notably, these spots often fail to produce any significant  $H_3^+$  emission (Stallard et al., 2016), with simultaneous JWST and HST observations showing the same noon active region enhancements more than doubling the UV emission brightness, while the  $H_3^+$  emission brightness by <10%.

This region was previously associated with the slow-moving middle magnetosphere, with ions significantly subrotating in this sector (Stallard et al., 2001). However, with recent observations showing the vortex within the auroral upper atmospheric forces neutrals to lag slightly slower than the slow moving ions, resulting in a weak antisunward  $\vec{E} \times \vec{B}$  drift in this region (R. Wang et al., 2023), perhaps indicating ions are being collisionally dragged by the neutral vortex generated by equatorward ion flows, or, alternatively, that the difference between ions and neutrals are produced by a weak antisunward  $\vec{E} \times \vec{B}$  drift in some way with the solar wind.

#### 1.3.3. Swirl Region

Closer to the pole on the dawn side, there is a region of weaker, highly variable emission known as the Swirl region (orange in Figure 1; Grodent, Clarke, Waite, et al., 2003). In the UV, the variability of this region on timescales of 1-2 min is so large, it is typically difficult to observe congruent features. However, over longer timescales of  $\sim 10$  min, the Swirl region generally has an extended arc of relatively bright emission along its dawn flank. Similar short-term variability is also observed by JWST in  $H_3^+$  emission (J. D. Nichols et al., 2025), but these emissions also show clear continuous structures. This is because of the extended lifetime of that ion (Stallard et al., 2016); while JWST showed that bright  $H_3^+$  features fade quickly in the Swirl region, recent Juno-JIRAM measurements of the Io spot have shown that  $H_3^+$  lifetime is inversely proportional to the  $H_3^+$  column density (Mura et al., 2025), so weaker features may sustain for significantly longer in the IR than the UV.

This polar region is strongly correlated with enhanced UV absorption in the atmosphere (a high UV color ratio), especially when contrasted against the surrounding auroral regions (Gérard et al., 2003), suggesting deeply penetrating high energy particle precipitation. It is in this region that JEDI has identified periods of particularly energetic (potentially >10 MeV) electron beams (Paranicas et al., 2018). This shows that the Swirl and Active regions map to very particle energy distributions, and so potentially very different surrounding space environments.

The emission in this region is also highly modulated across the day-night terminator, reducing significantly past the nightside terminator (Greathouse et al., 2021). Notably, when on the dayside, neither the brightness or color ratio of this high-color ratio core seems to vary consistently with local time in the limited number of observations so far published.

STALLARD ET AL. 6 of 24

Ions in this region strongly sub-corotate (Johnson et al., 2017; Stallard et al., 2001), appearing to be stagnant in the inertial frame, perhaps indicating control by the solar wind. However, recent simultaneous observations of ions and neutrals by R. Wang et al. (2023) showed that the ions are closely tied with the flow of the neutral auroral vortex. As with the Active region, this might indicate ions dragged by the neutral atmospheric vortex and/or a weak sunward  $\vec{E} \times \vec{B}$  drift in this region.

#### 1.3.4. IR Dark Pole Region

Over the magnetic pole,  $H_3^+$  emission often shows a region of darkening (green in Figure 1). A feature likely driven by differences in ion density, since temperatures in these regions are typically comparable to, or even hotter than, the surrounding pole (Johnson et al., 2018; Moore et al., 2017). However, a commensurate darkening is not typically seen in the UV (Stallard et al., 2016), and the source of these auroral differences is not currently well understood.

#### 1.3.5. Magnetic Origins of the Polar Aurora

The origin of these polar sub-regions remains controversial, with significant differences in interpretation of whether these regions are partially open to the solar wind (Cowley et al., 2003) or are entirely closed, linked to the planet's magnetospheric flanks (Delamere & Bagenal, 2013). More recently, different models have attempted to map magnetic fields between the surface of the planet and the surrounding magnetosphere, accounting for regions that appear to be open to the solar wind.

The most recent models of Jupiter's magnetic field (Connerney et al., 2018, 2022) utilize numerous Juno orbits to provide incredible details in Jupiter's surface magnetic field structure. However, away from the planet, these models become increasingly inaccurate with distance, because they cannot account for external influences, such as the magnetospheric ring current or the pressure of the Solar Wind. To account for such external influences, the internal field needs to be modeled for a specific central meridian longitude (CML), allowing the asymmetric distortion of the solar wind to be included.

The Vogt et al. (2011) model does this by mapping contours of constant radial distance by requiring the magnetic flux in each specified region of the magnetospheric equator equals the magnetic flux in the area to which it maps in the ionosphere. Vogt et al. (2015) quantified how this model changes for a range of magnetic field models, and the model has since been updated as recently as the JRM09 model, produced by Connerney et al. (2018). This generally maps the UV polar Dark region to the dawn flank of the middle/outer magnetosphere, the Active region to the dusk flank and the Swirl region onto field lines open to the solar wind, but it is worth noting the boundaries of these regions are not clearly defined, with each region varying significantly with magnetospheric condition, a variation not included in Vogt et al. (2011). The model also only outputs mapping from 15  $R_J$  to 150  $R_J$  in the equator (Jupiter's magnetic field strength means magnetic mapping does not change significantly with local time at distances <15  $R_J$ ).

In contrast with this, the Zhang et al. (2021) model uses magnetohydrodynamic modeling to simulate the interaction of the solar wind and interplanetary magnetic field with the Jovian space environment, following the changing mapping of dipolar magnetic field lines with the surrounding space environment as the planet rotates. This model reveals a polar region that is dynamic and unstable, with ionospheric location often flickering between mapped locations. However, by running the simulation across four entire planetary rotations, statistical averages were used to define three polar regions of preferential connection. The model predicts the first as a region of ionospheric open flux shifted to the dawnside, suggesting that a dawnside auroral feature like the UV dark polar region could be on open field lines. The second prediction is a duskward region of open magnetic lobe that spirals far into the magnetic tail, perhaps aligned with some of the duskward Active region. Finally, the model predicts a lobe of closed magnetic field that maps into the magnetospheric dawnside flank, perhaps aligned with Jupiter's Swirl region, but, notably, Zhang et al. (2021) state that some or all of the dayside Active region also falls into this region.

Notably, these two models disagree on which of these three auroral regions are predominantly open or closed, highlighting how poorly resolved are the drivers of Jupiter's polar aurora.

STALLARD ET AL. 7 of 24

High cadence observations of the UV emission by the Hubble STIS instrument has revealed the Swirl region emission actually results from ribbon-like auroral swirls that move sinuously across the entire polar auroral region (i.e., both the Swirl and Active region). These auroral swirls cover such a large range of magnetospheric mapped locations that the origin for these emission must come from close to the planet, rather than the equatorial magnetosphere (Grodent & Bonfond, 2014). Only one potential explanation for these emission structures currently exists: that these ribbons of auroral emission are driven by reconnection events close to the planet, unique amongst the planets because only Jupiter's very strong magnetic field strength is able to drive such reconnection (Masters et al., 2021). These are perhaps more akin to ribbon flares observed within the chromosphere of the Sun, an atmospheric layer similarly dominated by molecular neutrals, significant ion-neutral coupling strongly modulated by strong magnetic fields, and by varying Pedersen conductivity (Fletcher et al., 2011).

#### 1.4. Dominant Trends in Jupiter's H<sub>3</sub><sup>+</sup> Northern Aurora

In order to better understand the underlying trends in Jupiter's auroral brightness, a study preceding this investigation combined a huge data set of auroral images, originally taken by Jack Connerney and Takehiko Satoh between the years 1995–2000 (available at Stallard, 2018), to smooth out variability in the auroral brightness. That investigation, published as a companion paper to this work (Stallard et al., submitted), hereafter described as Paper I, discussed how each individual pixel in these images was mapped into planetary latitude, planetary longitude and planetary local time, producing a three dimensional array of ionospheric brightness. In doing so, short timescale variability typically observed on timescales between minutes and days, is diminished through the use of >13,000 images, taken over 48 observing nights and more than 6 years, revealing the underlying long-term auroral trends for the first time.

These trends can relate to changes within the ionosphere of the planet:

- 1. Varying in System III coordinates with the *planetary latitude* and *planetary longitude*, most dominantly as a result of Jupiter's magnetic field, locked by definition into this coordinate system;
- 2. Varying in *planetary local time*, most likely as a result of changing solar illumination, with solar EUV driving ionization in the upper atmosphere;

Similarly, trends in the aurora can also relate to changes within the surrounding magnetosphere:

3. Varying in the magnetic local time within the magnetospheric equatorial region that the ionosphere maps to. This is dominated by the solar wind influence on Jupiter's magnetosphere.

Paper 1 focused on the dominant trends in the ionosphere itself, revealing two clear trends in Jupiter's auroral region:

- 1. The  $H_3^+$  main emission brightness is strongly anti-correlated with surface magnetic field strength at a Pearson correlation of p = -0.904.
  - (a) This main emission anti-correlation is thought to result from a combination of effects. Firstly, the anti-correlation between magnetic field strength and Pedersen conductivity, detailed at Jupiter by Gérard et al. (2013). Secondly, the canceling effect of the strengthening of UV emissions for a given precipitation current with enhanced magnetic field strength (J. Nichols & Cowley, 2004). Thirdly and finally, a second anti-correlation because of enhanced surface magnetic fields resulting in a reduction in the coupled magnetospheric currents (Ray et al., 2014).
  - (b) Polar aurora occurs under too small a range of magnetic field strengths for a correlation to be measurable, but the expectation is that this aurora will also be anti-correlated. This is because they are driven by either diffuse auroral processes (in which case an anti-correlation will result from higher magnetic field strengths driving stronger magnetic mirror forces, preventing pitch-angle scattering into the atmosphere) or current driven precipitation processes (in which case the polar aurora undergo comparable anti-correlations to those in the main aurora).
- 2. The H<sub>3</sub><sup>+</sup> main emission brightness is strongly correlated with planetary local time and peaks closest to noon, at a Pearson correlation of 0.93 between the main auroral emission brightness and the best fit of H<sub>3</sub><sup>+</sup> brightness from the EUV ionized non-auroral regions on Jupiter. This correlation is also believed to originate from Pedersen conductivity, with past modeling by Tao et al. (2010) showing that solar ionization driving

STALLARD ET AL. 8 of 24

significant enhancement in the main auroral emission, which matched well with the overall variation observed in Paper I.

• This is particularly noteworthy as it implies the magnetospheric source of precipitation is strongly influenced by the conditions within the ionosphere. Pitch angle scattered precipitation should not be influenced by the conditions of the ionosphere it is falling into, while discrete currents closing through the ionosphere are highly dependent of the ionospheric conductivity. Since only 7% of precipitation results from discrete acceleration, this again highlights that it is the breakdown-in-corotation that drives auroral brightness, most probably by enhancing broadband pitch-angle scattered precipitation by scaling the extent of instabilities in the particle population above the planet.

Paper I was also able to reveal two poorly constrained trends. Firstly, there appeared to be additional secondary planetary local time variations between dawn and dusk, suggesting additional trends driven by morphological complexity not resolved in the broad auroral averaging of Paper I. Secondly, the polar regions showed very poor correlation with planetary local time, suggesting strong morphological controls on the brightness variations across this region.

Here, we further explore the data set introduced in Paper I, removing the dominating trends of magnetic field strength and planetary local time in order to mine the latitude, longitude and planetary local time datacube to reveal the underlying morphological variations with both planetary and magnetic local time.

#### 2. Data Mapping

We follow both Paper 1 and Stallard et al. (2018) in utilizing the extensive data set of observations taken to produce the Connerney et al. (1998) VIP4 model observed Jupiter over a period of 5 years using the NSFCAM imager on NASA InfraRed Telescope Facility on Mauna Kea, Hawaii (Shure et al., 1994). Over 48 individual observing nights, more than 13,000 individual images were taken (available at Stallard, 2018), with the only strong biases in observational timing being focused on times when Jupiter was close to opposition, and when Io was on the dayside of the planet (so that an Io spot could be observed). These utilized a range of high-resolution filters tuned to observe  $H_3^+$  at wavelengths between 3.42 and 3.46 and 3.53  $\mu$ m, over a field-of-view of 37.9 arcsec (with the 256 × 256 pixel array providing a pixel scale of 0.15 arcsec), just too small to fit Jupiter entirely into the frame. An example image is shown in Figure 1.

Since the precise filter distributions are not currently available, we cannot measure absolute intensities, relying instead upon the same assumptions presented in both Paper 1 and Stallard et al. (2018) to produce a relative  $H_3^+$  emission brightness. This normalization to the mean auroral emission brightness is a direct ooutput from the factorization of Jupiter's auroral brightness relative to magnetic field strength detailed in Paper 1, and described below.

The data set of observations (available at Stallard, 2018) taken to produce the Connerney et al. (1998) VIP4 model provides a unique level of longitudinal coverage, and across all dayside local times. As with Paper I, and unlike Stallard et al. (2018), we map individual image pixels into latitude, longitude and planetary local time, summed across the data set.

Figure 2 shows the same view of the northern and southern hemispheres as highlighted in Figure 1 in Paper I, but here, we have restricted the data to planetary local times in the dawn sector, between 07:00-09:00. We have projected this map into a northern and southern polar projection (Figures 2a and 2b) and an cylindrical projection (Figure 2c). Secondly, we combine emission across all longitudes, to produce a normalized cylindrical map of local time versus latitude (Figure 2d). Finally, we combine emission across all latitudes, to produce a normalized cylindrical map of longitude versus local time (Figure 2e).

This produces maps of the average intensity summed over this local time range. Despite the reduction in total integration time caused by narrowing our parameter space (down to only 20–40 hr per pixel across 15–30 days within each of the five local time sectors), the northern auroral region remains well displayed, with clear structure. Unfortunately, the southern auroral region is not well resolved, drastically affected by strong noise issues that results in data poleward of  $\sim 70^{\circ}$  of Jovigraphic latitude having too many artifacts to be usable. Since this encompasses the majority of the auroral region within the southern auroral region, we will restrict our analysis of the effects of changing local time to the northern auroral region, where a combination of the higher integration times

STALLARD ET AL. 9 of 24

(so that artifacts appear poleward of 80° Jovigraphic latitude) and the greater offset between the Jovigraphic and Jovimagnetic poles allows us to accurately observe most of the auroral region.

One apparent issue with this mapping is there are the significant striations seen when the data is plotted in longitude-local time, shown in Figure 2e). The harsh striations in that panel are dominated by variability produced by combining brightness values from a wide range of latitudes, blending equatorial emission with auroral. When plotting only a narrow range of binned latitudes, this striation is significantly reduced (as shown in the Supporting Information S1), but the natural variation in our data does still provide some weaker errors.

In Paper I, this striation was not an issue, since correlations in the data were compared across the sum of a large number of latitudes and longitudes. In this paper, we intend to explore the latitude and longitude morphological variations across a range of planetary local times, and so in order to understand variations in emission structure and brightness with local time, and smooth out these narrow striations, we will sum our measured emission across five local time sectors: 08 hr (07:00–09:00), 10 hr (09:00–11:00), 12 hr (11:00–13:00), 14 hr (13:00–15:00), and 16hr (15:00–17:00). These bins are chosen specifically because they are larger than the length of the observed striations.

Since only relative brightness is available in this data set (Stallard et al., 2018), and so we re-scale the brightness to the median brightness of the  $H_3^+$  aurora in the region that maps (according to Vogt et al. (2011), using Connerney et al. (2018)'s JRM09 model) to between 20  $R_J$  and 80  $R_J$ , across all local times between 07 and 17 hr.

One aspect of the Jovian aurora that has proven confusing in interpreting our analysis is the degree to which we are biased toward terminology ingrained over two decades of explaining auroral emissions taken from the same close-to-noon planetary local times. In our experience, it is easy when discussing auroral features to fall back into describing the western curved section of the main emission as the "dawn" emission, and the eastern kinked section as the "dusk" emission. To resolve this, we here define four "regions" within the northern main emission, describing four quarters of the emission, named for letters that approximate the overall shape of northern auroral morphology: Regions A, V, C, and D, each representing a quadrant of magnetic longitude radiating from the northern magnetic pole. For convenience, we use the conventions of magnetic latitude and longitude laid out in Grodent, Clarke, Kim, et al. (2003), with the northern magnetic pole positioned at 75°N and 175°W. We highlight the location of these four regions in Figure 2a in pink:

Region-A: The somewhat sharply pointed narrow end of the oval closest to the rotational pole. This region is largely ignored in this study, as it falls close to the rotational pole and thus is poorly resolved from Earth, ranging between magnetic longitudes of  $315^{\circ}$ - $45^{\circ}$ .

Region-V: The most sharply pointed equatorward-most region of the aurora between the kinked and unkinked part of the oval. This region ranges between magnetic longitudes of 135°–225°.

Region-C: The unkinked, western part of the oval, forming a broadly circularized C shape when seen from above. In past papers describing the aurora from Earth-based observations, this has typically been named the "dawnside" aurora. This region ranges between magnetic longitudes of 225°–315°.

Region-D: The kinked, eastern part of the oval, forming an approximately straight line on the globe of Jupiter when seen from above, that causes the entire auroral oval to be broadly D shaped. Past Earth-based observational papers typically named this the "duskside" aurora. This region ranges between magnetic longitudes of 45°–135°.

#### 2.1. Selecting Different Local Time Phases

Our understanding of the auroral structures at Jupiter are highly biased toward observations made from Earth. Even when viewing Jupiter at quadrature, the maximum range of Earth-Jupiter-Sun angles possible is only  $\sim 10^{\circ}$ , preventing any views of the nightside ionosphere and aurora. However, as the planet rotates, it is possible to compare and contrast the aurora across the entire dayside, between 06 UT and 18 UT.

We avoid emission that sits very close to the limb of the planet (using emission <0.98 of the limb distance), where errors in the limb-brightening could become significant, and map the emission in the 2-hr local time bins discussed above, ranging between 07:00 (an hour after dawn) to 17:00 (an hour before dusk). These image maps are scaled to the mean brightness of the five sectors combined, resulting in consistent relative brightness across the

STALLARD ET AL. 10 of 24

five local time sectors. Using this methodology, it is possible to produce maps of the northern auroral intensity over a range of local times.

Figure 3 shows the resultant northern auroral emission across these five bins of planetary local time. Notably, here, we have yet to correct for the biases described in Paper 1, and so planetary local time and magnetic field strength strongly influence the resultant intensities. In Figure 3a, the first column of shows local-time-limited maps of average intensity mapped from above the northern auroral region. In order to highlight the brightness differences revealed by this relative scaling, Figure 3b, the second column, shows these local time limited maps of average intensity divided by the normalized average emission map across all local times between 07:00 and 17:00, to produce maps of the variation in local time intensity away from the mean. Figure 3c, the final column of the figure, is a cartoon view of the slice of individual images used to construct each image, using the data from all five sectors, with the planetary image located at a CML of 180. This highlights the strip of data used from each image that contributes to the maps in this figure.

Away from the rotational pole, each local time sector typically contains between 25 and 50 hr of integration from across the five years of this data set. Similarly, other than at the northern rotational pole, each local time sector contains emission from approximately 15-30 individual nights. Past analysis of Jupiter's infrared aurora (using this data set) revealed that the overall morphology of the  $H_3^+$  aurora appears to change slowly over an individual night of measurement, but will usually change significantly between nights (Stallard et al., 2016). These observations are clustered into 6 extended periods of observation over each of the 6 years the data set were taken, and so even accounting for periods of relative quiescence in the auroral morphology, the large number of individual observational days (15–30) and integration hours (>25) in each sector will act to smooth out the effects of short term drivers of the Jovian aurora.

#### 2.2. Observed Morphology Within the Planetary Local Time Sectors

Given the significant intensity differences seen in each local time sector, it is important to be clear that these variations are the result of viewing angle differences, rather than the significant variability that is often observed in the auroral emission on a night-by-night basis (Stallard et al., 2016). Each local time sector displays emission that is easy for viewers (the authors included) to interpret in comparison with images, but our experiences of interpreting images comes from Hubble and ground-based imagery (and now a range of Juno measurements), where each individual image covers a range of local times.

However, although these sectors provide information tightly constrained in planetary local time, they each access a differing range of magnetospheric local times, as the field lines map into surrounding space non-linearly as the offset auroral magnetic field lines flare up and outwards away from the planet (later highlighted in Figure 5). This mapping changes as stretched field lines mapping beyond  $\sim 50 \, R_J$  start to change their planetary location with magnetic local time. This variation has been modeled in detail by Vogt et al. (2011), with the most recent iteration of this model, combining the JRM09 magnetic model with calculations of the stretching of field lines out into space. Figure 3 shows the location of this mapping for  $30 \, R_J$ ,  $80 \, R_J$  and  $130 \, R_J$ , in blue, orange and green respectively (with these lines of mapping ending abruptly where the calculated mapping moves onto open field lines).

The width of the auroral emission is dominated by the mapped locations of magnetospheric regions into the planet. The projected magnetic mapping from the Vogt et al. (2011) model highlights the forcing together of magnetic mapping linked with the dawn magnetosphere, and drawing apart of magnetic mapping stretching into the dusk side of the magnetosphere. As we will see later, because these local time sectors are specifically within the planetary local time frame, there is a complex relationship between each of these sectors and the magnetospheric local times they relate to.

In Figure 3, on the dawn side of the planet (in 08 hr), Region-C maps tightly into the dawn sector, with the narrow auroral arc closely matching the very confined magnetic mapping, and Region-D spread out, matching the broad mapping in the dusk and midnight sections. Moving through planetary local time through to dusk, at 16 hr, the width of both the emission and the mapping is much more balanced on each side of the aurora. This strongly suggests the historic view that dawn aurora produces a tight auroral arc when compared with the dusk is at least partially an artifact of the uniquely narrow mapping observed only in Region-C in the dawn sector. Region-C is more widely spread at other local times, and dawn emission is more broadly spread away from Region-C.

STALLARD ET AL. 11 of 24

from https://agupubs.onlinelibrary.wiley.com/doi/10.1029/2025JA034076 by NICE, National Institute for Health and Care Excellence, Wiley Online Library on [16/10/2025]. See the Terms

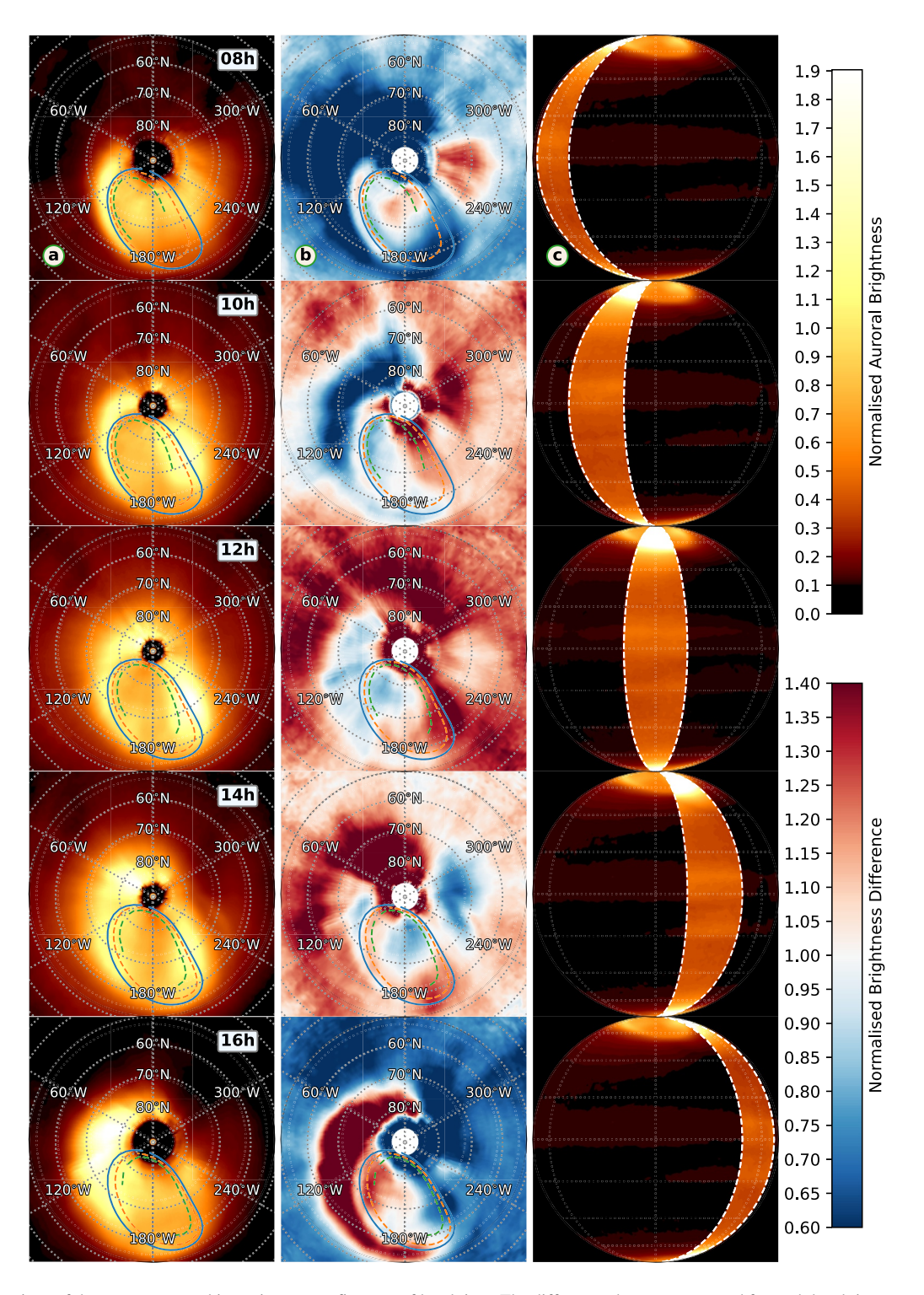


**Figure 3.** Polar projections of the average auroral intensity, across five sets of local time. The different values are presented for each local time range in rows, with the following local time ranges: 0.8 hr (07:00-09:00), 1.0 hr (09:00-11:00), 1.2 hr (11:00-13:00), 1.4 hr (13:00-15:00), and 1.6 hr (15:00-17:00). Column (a) shows the average intensity measured for that local time range, as shown in Figure 2a. This intensity range is fixed across the data set, with a gamma stretch of 0.5. Magnetic fields that map to the distances  $3.0 \text{ R}_J$ ,  $8.0 \text{ R}_J$  and  $13.0 \text{ R}_J$  in the most recent version of the Vogt et al. (2011) magnetic field mapping (that includes the JRM09 Connerney et al. (2018) model) are shown in blue solid, orange dashed and green dashed lines respectively. Column (b) shows the average intensity for each individual local time range divided by the average intensity across all local times, revealing regions where each local time is weaker (blue) or brighter (red) than on average. Column (c) shows a cartoon orthographic projection of Jupiter, providing a visual representation of the section of images used to produce each subset between (a) and (e). Notably, though, the auroral position (and longitude) is free to rotate through this local-time window.

STALLARD ET AL. 12 of 24

We note a potential viewing angle artifact within the most extreme local times, potentially arising from a combination of seeing and the altitude of the auroral column beginning to obscure surrounding regions. This is particularly strong when these adjacent regions are dark. At dawn, in 08 hr, this is strongest as the aurora rotates into view, scattering light westward from Region-D. At dusk, in 16 hr, it scatters light eastwards beyond Region-C. While this strong enhancement might be real, neither Juno's JIRAM images (Gérard et al., 2018; Mura et al., 2017) or more extensive UVS images (Greathouse et al., 2021) appear to show this.

However, perhaps such interpretation is overly cautious, since recent  $H_3^+$  observations by the JWST have revealed a very strong dusk brightening in Region-D, by far the brightest auroral feature at that time, with no comparable UV emission(J. D. Nichols et al., 2025). Perhaps such enhancements are intermittent, and so missed by JIRAM, but still observed regularly enough to translate to a strong enhancement on average within this region.

This scattering effect appears strongest in sub-auroral regions equatorward of the main emission, and so we focus in this study on the main aurora and polar emission. Across most local time sectors, there is also significant scattering in the most rotationally poleward regions, which will be ignored where our data become less dense with the following investigations.

#### 2.3. Variations in Auroral Morphology With Changing Planetary Local Time

Since polar emissions are expected to be dominated by magnetic field lines that map to either the edges of the magnetosphere or are open to the solar wind, while regions equatorward of this will map to a range of closed field lines within the middle magnetosphere, we will consider the main auroral emission and polar emission in two separate ways.

#### 2.3.1. Polar Auroral Morphology With Changing Planetary Local Time

In order to better understand the potential drivers for the polar enhancements in emission, we compare the measured brightness differences with the three polar auroral regions identified in the Zhang et al. (2021) MHD model. Despite the axisymmetric nature of that model, the instantaneous coupling within the auroral regions varied dramatically, with sporadic variations in the positioning of open field. However, when run over a period of four full planetary rotations, three different polar regions were identified as occurring regularly within the model. The three regions consisted of: (a) a region of field lines newly opened to the solar wind forming a crescent inside the main auroral emission region, rolling around the pole between noon, through dawn and midnight, ending close to dusk; (b) a small region of old open field lines representing a core of twisted field lines extending into the tail, a Jovian equivalent of the old core suggested at Saturn (Milan et al., 2005); and (c) a central closed region, inside these open field lines, which connects with the dawn region, close to the magnetopause.

To compare these regions with our statistically-averaged emission (which should, in theory, be dominated by the same three regions, since we have averaged over so many nights of observation), we adjust the published locations from the axi-symmetric Zhang et al. (2021) model so that they fit within the asymmetric northern auroral oval, as shown in Figure 4.

We firstly caution that the act of interpolating an axisymmetric dipolar model into a non-axisymmetric high order magnetic coordinate is a significant simplification, but it does allow us a test of the broad-level findings of such a model. Each region in the axisymmetric model approximately relocated into Jupiter's asymmetric northern auroral oval by stretching or contracting its position relative to the distorted shape of the  $40 R_J$  mapped location (changing the dipolar circular shape from Zhang et al. (2021) into Jupiter's asymmetric northern auroral shape) and a central pole location of  $72^\circ N$  and  $180^\circ W$  (approximately the center of the auroral region):

- 1. Firstly, we (for convenience) take the ionospherically-mapped location of the JRM09 variant of the Vogt et al. (2011) model at  $40 R_J$ , and remap the latitude and longitude positions using a polar transformation, so that the new pole is positioned at a central pole location of  $72^{\circ}N$  and  $180^{\circ}W$ .
  - the latitude of these remapped 40 R<sub>J</sub> locations provides a measure of the distortion away from a circle, a ratio of each latitude compared with the mean latitude of all remapped 40 R<sub>J</sub> locations, with some positions compressed toward the pole and some expanded toward the equator.
  - (NB: For convenience we have included the small change in the Vogt et al. (2011) model's 40 R<sub>J</sub> ionospheric mapping at each CML position, due to the changing solar wind angle, though again, these

STALLARD ET AL. 13 of 24

from https://agupubs.onlinelibrary.wiley.com/doi/10.1029/2025JA034076 by NICE, National Institute for Health and Care Excellence,

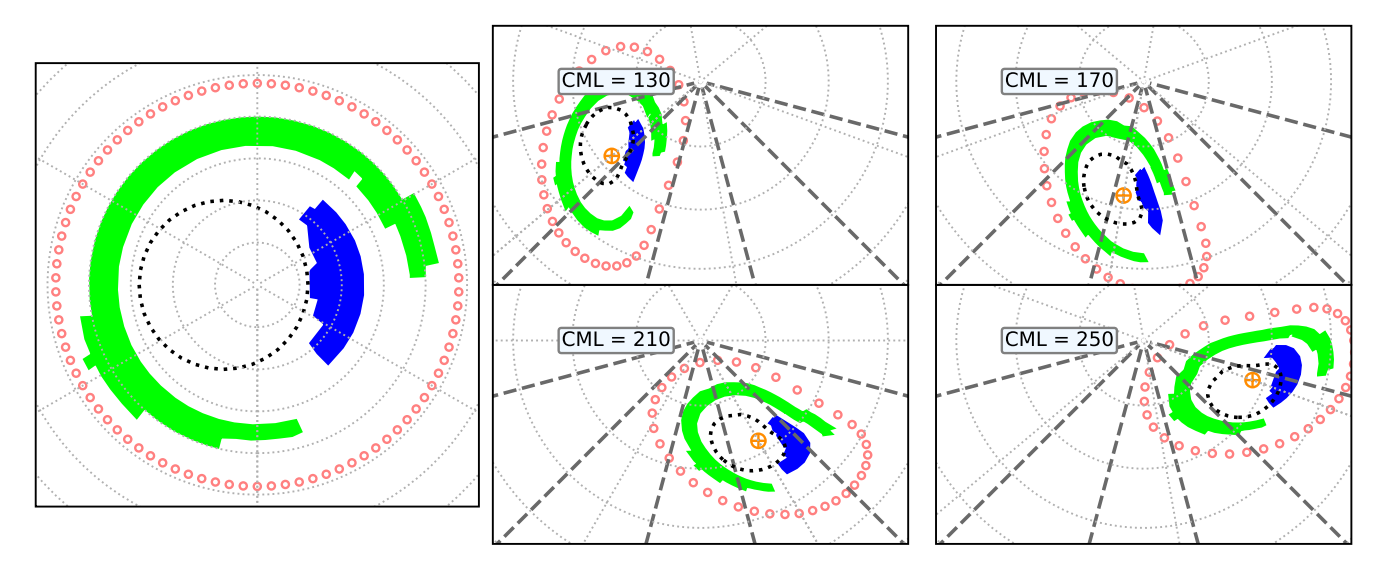


**Figure 4.** The polar regions from the Zhang et al. (2021) model distorted into Jupiter's asymmetric auroral morphology. On the left, we show a polar map of the regions described in the axisymmetric dipolar Zhang et al. (2021) model: the partial torus of open field lines (green), the small duskward core of old field lines extending down into the magnetic tail (navy), the central approximately circular region closed polar region, mapping to the dawnside outer magnetosphere (black dots) and  $40 \, R_J$  (red circles; all panel line styles match with those in Figure 4 of Zhang et al., 2021). One the right, we show four panels, each at a different central meridian longitude, each showing our approximation of how these regions would appear distorted into Jupiter's asymmetric magnetic field. Here, the  $40 \, R_J$  mapping (red circles) is instead taken from the JRM09 version of the Vogt et al. (2011) model, and we also show the central auroral location (orange plus within a circle;  $72 \, ^{\circ}N$  and  $180 \, ^{\circ}W$ ), both used to produce these approximate locations. The location of the five local time sectors (black dashed lines) used in this study are also show, for comparison.

regions should not be taken to be exact, or a true mapping, due to the significant assumptions used in this shifting).

- 2. Secondly, we use these transformed  $40 R_J$  positions as a proxy for the Zhang et al. (2021)  $40 R_J$  locations (in reality Zhang et al. (2021) would differ in true location from Vogt et al. (2011), but for a positional approximation, the assumption these match is reasonable).
  - (a) for a given "remapped magnetic longitude," the distorted  $40 R_J$  location tells us the extent to which each Zhang et al. (2021) region's latitude in that longitude sector should be compressed or expanded to match with that distortion.
  - (b) repeating this transformation across all remapped magnetic longitudes, we calculate the distorted latitude and longitude shape of each of the Zhang et al. (2021) regions around the shifted pole.
- 3. Finally, we polar transform these distorted Zhang et al. (2021) regions back to the rotational pole coordinates.

Since the three polar regions in Zhang et al. (2021) are fixed in local time, the distorted shape of these regions changes with CML, as the three regions are squeezed and stretched into the northern auroral shape in the direction of the Earth. We provide a video highlighting this distortion as seen from Earth in the Supporting Information S1.

Paper I highlighted the two strongest influences on Jupiter's  $H_3^+$  main auroral intensity structure: (a) the inverse proportionality of the surface magnetic field strength to  $H_3^+$  emission brightness; and (b) the proportionality of the overall auroral brightness to planetary local time. In order to reveal underlying morphological changes, we now apply two corrections to the data to account for these dominant trends:

- 1. The anti-correlation between the JRM33 magnetic field strength (Connerney et al., 2022) and  $H_3^+$  main auroral emission brightness is accounted for by dividing brightnesses by the best fit second-order polynomial fit of this correlation, using the values:  $B_0 = 1,120.57$  and  $B_1 = -43.6417$ .
- 2. The correlation between planetary local time (in hr) and  $H_3^+$  main auroral emission brightness is accounted for by dividing brightnesses by the best fit fourth-order polynomial with the values:  $LT_0 = -7.1767 \times 10^{-6}$ ,  $LT_1 = 1.945 \times 10^{-6}$ ,  $LT_2 = -8.3156 \times 10^{-8}$  and  $LT_3 = 3.189 \times 10^{-6}$ .

Figure 5 shows the same five local time sectors highlighted in Figure 3, but here corrected for magnetic field strength and the changing overall brightness associated with planetary local time. This allows a clearer comparison within both the main auroral emission and polar regions. At 08 hr, although the emission is brighter than

STALLARD ET AL. 14 of 24

2169402, 2025, 10, Downloaded from https://agupubs.onlinelibrary.wiley.com/doi/10.1029/2025/A034076 by NICE, National Institute for Health and Care Excellence, Wiley Online Library on [16/102025]. See the Terms

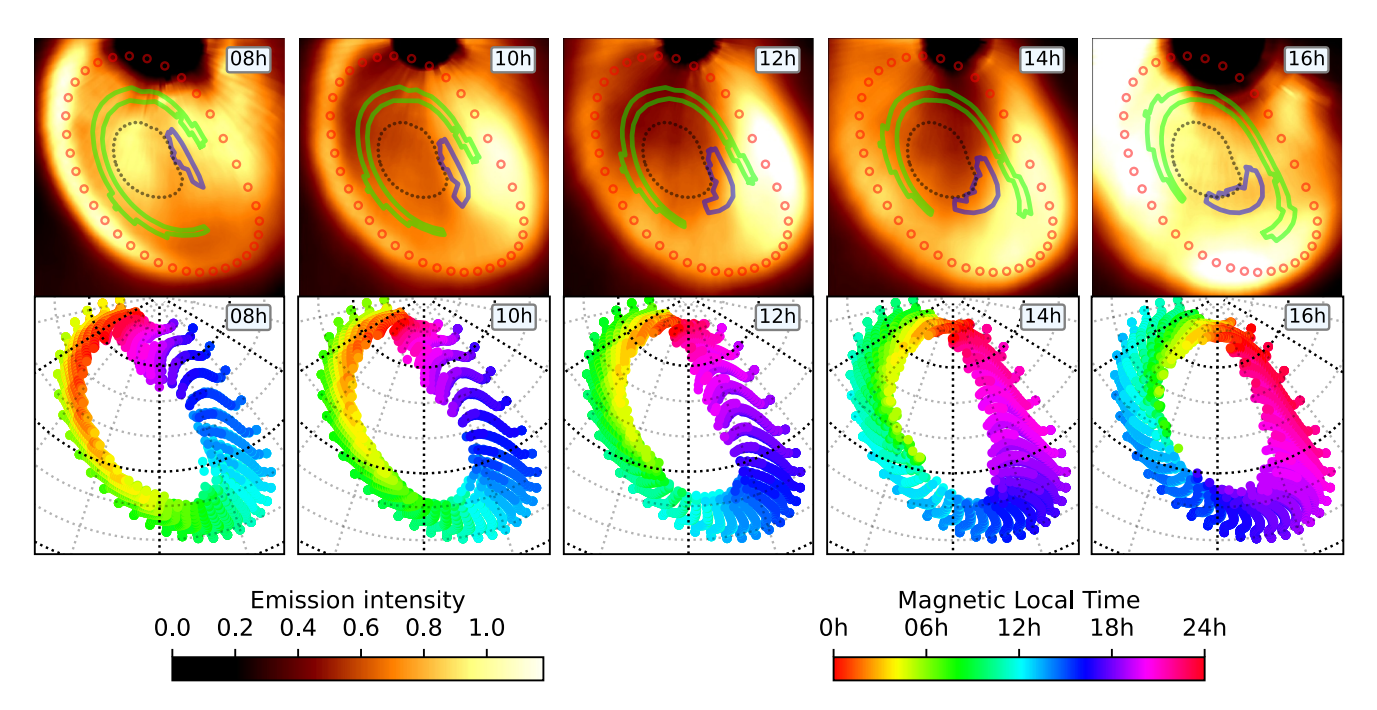


Figure 5. Scaled auroral emission brightness compared with magnetic mapping. In the top five panels, each of the five planetary local time sectors outlined in Figure 3 have been corrected for magnetic field strength, using values fitted in [the companion paper]. Overlain on these are the magnetic field mappings from Vogt et al. (2011) for  $40R_J$  (red circles). Also overlain are the three polar regions discussed in Zhang et al. (2021), reformed from circularized magnetic latitude into the magnetic morphology of the JRM09 model mapping from Vogt et al. (2011), using the shared magnetic position for  $40R_J$  from both models as a guide. These three Zhang et al. (2021) regions are the partial torus of open field lines (green), the small duskward core of old field lines extending down into the magnetic tail (navy) and the central approximately circular region closed polar region, mapping to the dawnside outer magnetosphere (black dots; all panel line styles match with those in Figure 4 of Zhang et al., 2021). Notably, these two models disagree on the regions of open and closed magnetic field mapping to regions beyond  $\sim$ 80  $R_J$ ; these top panels provide an indication of mapping distance from the planet for the two models, but not what local time these map to. In the second row, we show the magnetospheric local time the auroral region magnetically maps to, according to the Vogt et al. (2011), with individual points demarking planetary distances between 15  $R_J$  and 150  $R_J$  in 5  $R_J$  steps, and 10° steps in longitude. Here, we overlay dotted lines showing latitude (black in steps of 15°N) and gray in steps of 5°N) and longitude (black in steps of 60°W and gray in steps of 20°W), with all maps plotted with 180°W at the bottom.

more noonward sectors, the morphology of the polar emission appears to match well with the projected polar morphology of the Zhang et al. (2021) model.

- Inside the polar edge of Region-C of the auroral oval is a thin slice of darker emission this is the same "Dark" polar region described above.
- The "Swirl" region is revealed as a bright region of infilled emission over the most poleward regions, aligning with closed field lines stretching onto the morning side. Past auroral morphology has highlighted that this region is often bounded by an arc of emission on the dawn side (e.g., Stallard et al., 2016), though this is not visible here.
- Toward Region-D, the Active region is not as obvious here, but there is some polar enhancement, but there is certainly no evidence of the Polar dark region often seen in H<sub>3</sub><sup>+</sup> images. Indeed, this region is locally bright, perhaps aligning with the predicted location of Zhang et al. (2021)'s old core of twisted open field lines.

In this most dawnward configuration, the Region-D main aurora has extended regions that are closed, mapping to the post-noon middle magnetosphere at distances  $<150 \,\mathrm{R}_J$ , while the Region-C aurora is very tightly confined. This asymmetry in the main auroral width, combined with the polar auroral structures, make this 08 hr sector the most recognizable in comparison with typical Earth-based auroral imagery (Stallard et al., 2016).

Moving duskward, the auroral regions change in morphology with planetary local time, with the clearest changes in brightness being observed in the Dark and Swirl regions of the pole. The Dark region appears to move with local time, between 08 and 16 hr:

• The Dark region rotates from Region-C toward Region-A from dawn to noon, then from Region-A toward Region-D toward dusk. This is a largely geometric effect, the result of always mapping our data at a CML of

STALLARD ET AL. 15 of 24

180, and more strongly aligns this darkening with Zhang et al. (2021)'s true open field line crescent, since this region also rotates around with the planet. As shown in Figure 4, the open field line region is always dusk-aligned when observed from the Sun and Earth, but here, they move, as 180°W (and our field of view) rotates with the planet, relative to the Sun. However, it is notable that the Dark region does seem to move faster around the planet than the predicted open field line region, suggesting this is more than just a geometric effect and may indicate the distorted shape of Jupiter's magnetic field may influence the magnetospheric origin of the Dark region.

The polar region closest to Region-V remains relatively bright throughout the rotation of the auroral oval from
dawn to dusk, except perhaps at dawn. Notably, the polar Region-V is only co-located with the open field line
crescent in the first dawn panel, suggesting the emission brightness here aligns also with the predicted location
of our remapping of Zhang et al. (2021)'s open field line region. It might also indicate the rotation of the Active
region from Dawn to Dusk.

In contrast with this, the 'Swirl' region changes in brightness and morphology significantly with local time:

- The bright emission at dawn is not seen again until dusk, though at dusk the emission structure is very different, without an observable boundary between this region and the main auroral oval. If this region is colocated with the predicted location of Zhang et al. (2021)'s closed field line dawn magnetopause region, it suggests a dramatic change in the nature of this ionosphere-magnetosphere interaction, resulting in significant precipitation at dawn and dusk and much weaker precipitation closer to noon.
- Alternatively, the significant changes in emission observed here might indicate a fundamental change in the
  magnetic source region for the Swirl region with local time, suggesting the complexity of Jupiter's magnetic
  field fundamentally changes the locations of ionospheric mapping when compared with the axisymmetric
  Zhang et al. (2021) model.

Finally, all polar regions brighten most at dusk, suggesting significant enhancements in polar emission as the aurora rotates into the duskward direction.

#### 2.3.2. Main Auroral Morphology With Changing Planetary Local Time

While distorting the Zhang et al. (2021) regions into Jupiter's asymmetric shape provide us with hints to the potential sources of Jupiter's polar auroral structures, in regions closer to the main emission, closed field line region are much more accurately investigated with a detailed model of magnetospheric mapping. The bottom row of Figure 5 compares the emission maps with the locations of magnetospheric local time provided by the JRM09 variant of the Vogt et al. (2011), mapped out in steps of 10 degrees of longitude and 5 R<sub>I</sub> respectively.

These highlight that individual slices of planetary local time actually map out a wide array of magnetic local times, and that this mapping is complex, changing significantly for similar magnetic longitudes on the planet, as the mapped field lines access very different locations within the magnetosphere. This effect is most notable in the magnetic mapping shown across most planetary local times in Figure 5 as a red "spiral" of close-to-midnight magnetic local times that extends from Region-A, through Region-C along the westward edge of the oval toward Region-V. This showcases how small changes in magnetic latitude result in stark changes in magnetic local time, having a much higher impact on the magnetic mapping than the planetary local time. As such, planetary local time provides a poor measure of magnetic local time, especially in the northern hemisphere, and the only way to effectively account for this local time complexity is to use the magnetospheric mapping from models like the Vogt et al. (2011) model.

#### 2.4. Variations in Auroral Morphology With Changing Magnetospheric Local Time

Since magnetic local time varies on small scales across the auroral region as a function of planetary local time, latitude and longitude, understanding the changing auroral emission with magnetospheric location is somewhat non-trivial, especially since we also want to correct for the changing effects of magnetic field strength and planetary local time on emission brightness. As a compromise to this complex problem, we will apply the corrections to each of the five planetary local time sectors, as seen in Figure 5. For each planetary local time sector, a different latitude-longitude to magnetic equator mapping is needed, as the magnetic field lines are distorted away from the planet's surface by the solar wind. By calculating the magnetic mapping in each individual planetary

STALLARD ET AL. 16 of 24

from https://agupubs.onlinelibrary.wiley.com/doi/10.1029/2025JA034076 by NICE, National Institute for Health and Care Excellence, Wiley Online Library on [16/102025]

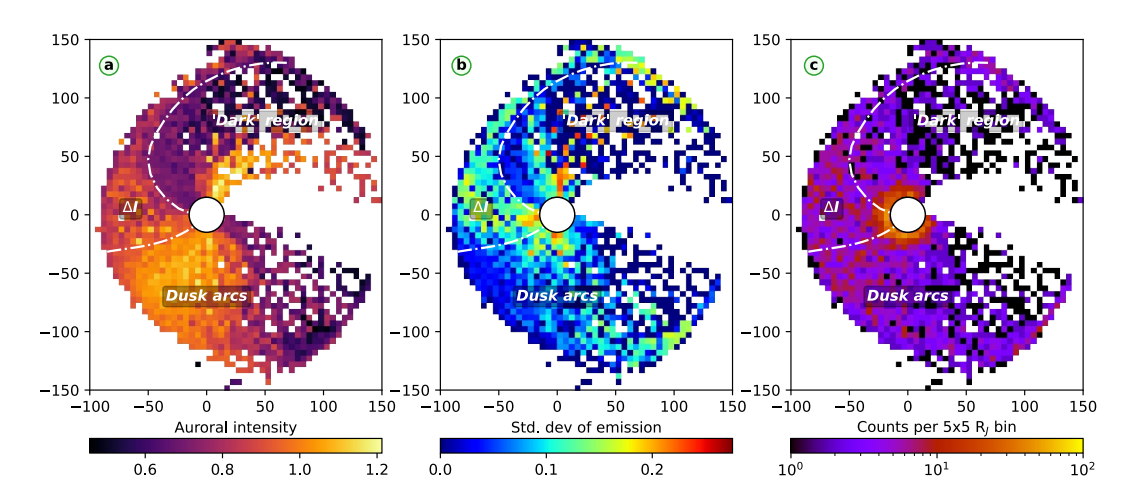


Figure 6. Magnetically mapped auroral emission brightness, standard deviation and count numbers. All three panels show the x and y plane of the Jovian magnetosphere in Jovian radii, with x and y axes pointing parallel and perpendicular with the Sun respectively. The Sun is located to the left, with the xy position showing the equivalent to magnetic local time, with noon (12 UT) to the left, dusk (18 UT) to the bottom, midnight (00 UT) to the right and dawn (06 UT) to the top. The left panel shows the mean auroral emission from the five sectors mapped into magnetospheric coordinates. Individual pixels in each sector map are assigned a magnetic local time and planetary distance using a nearest neighbor comparison with the mapped coordinates shown in Figure 5, and are then binned into  $5 R_J^2$  regions to produce a mean intensity surrounding the planet. Different regions see significant variation in the standard deviation of the pixel brightness mapped into that region, shown in the central panel, with total numbers of pixels contained within each  $5 R_J$  bin shown in the right. Three regions are delineated in each map. The bright "Dusk arc" region represents brighter emission associated with the Region D emission typically observed on the dusk side of the aurora from Earth. The "Dark" region magnetically maps into the polar region just inside the main emission, typically observed from Earth on the dawn side, equatorward of the "Swirl region." Between these region is a sector near magnetic noon that is very enhanced in standard deviation, suggesting significant variability, that has been labeled "ΔI."

local time bin, we can, in principle, transpose from the specific latitudes and longitudes at a given planetary local time, to reveal the magnetospherically induced auroral structures.

We map the emission in these five sectors out into the magnetosphere using the Vogt et al. (2011) model. Vogt et al. (2011) provides this changing mapping in steps of  $10^{\circ}$  CML (with the CML acting as a proxy for the changing planetary local time here), and so for each individual pixel in the map, we apply a linear interpolation of the calculated Vogt et al. (2011) model values for all the magnetic local times contained within each sector, to interpolate between the closest sets of local time and distance values at latitudes and longitudes given by the model. This allows us to produce an irregularly gridded set of magnetic local times and distances, consisting of each pixel in each planetary local time sector, each with an emission brightness. This emission is then gridded into magnetospheric local time and planetary distance with a  $5 \times 5 R_J$  gridding. Figure 6a shows the resultant mean emission projected into the magnetosphere, Figure 6b shows the standard deviation around that mean value, and Figure 6c shows the data density for each of these map positions, the number of pixels filling each grid point.

Within the average maps of magnetospheric mapping, three clear regions can be seen. The first is the strong enhancement in the dusk side emission, associated with the broad arcs of  $H_3^+$  emission seen in Juno observations of the aurora (Gérard et al., 2018).

The second is the much darker region on the dawn side, perhaps associated with the "Dark" region in the pole, but seeming to extend inwards toward the main auroral region. Notably, Figure 6a shows the dusk brightened region is approximately three times brighter than the "Dark" dawn region. This correlates very well with the prediction of Bonfond et al. (2015), who noted that the southern UV emission was enhanced in the dusk sector compared with dawn, but that the northern UV emission was more balanced. Bonfond et al. (2015) predicted that a factor of three enhancement would exist in both hemispheres, and that the apparent balance seen in the northern aurora was mitigated by that hemisphere's more complex magnetic fie;d structure. Here, we confirm that the hemispheric difference is the result of the strong magnetic field variation in the northern auroral region.

The final region, appearing as a speckled region in intensity is very clear within the map of standard deviation, as a noon slice with much larger variations in intensity than surrounding areas. This " $\Delta$ I" region is not a region of poor

STALLARD ET AL. 17 of 24

nlinelibrary.wiley.com/doi/10.1029/2025JA034076 by NICE, Nationa

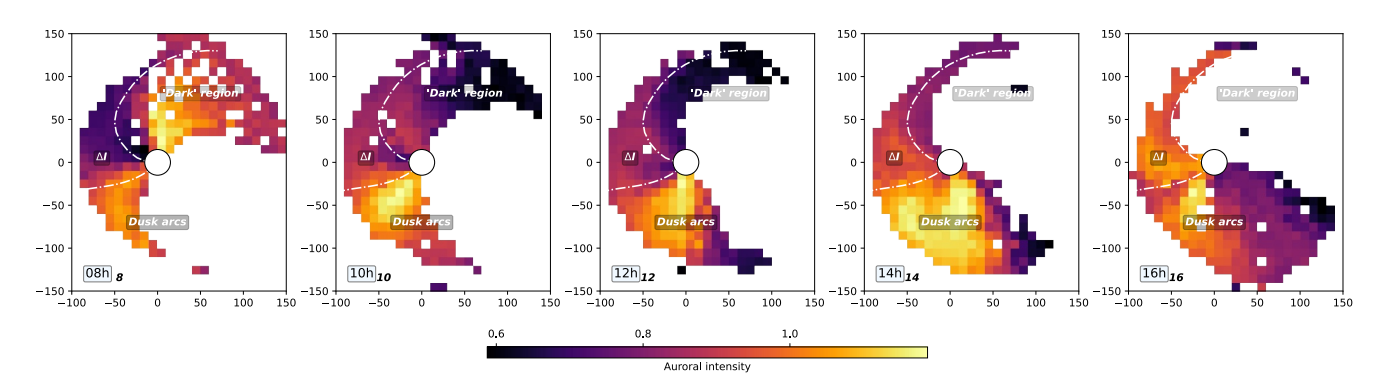


**Figure 7.** Magnetically mapped auroral emission brightness for each local time sector. Each panel shows the individual mapped image described in Figure 5, highlighting the changing auroral brightness for each sector, the average for which is the combined emission shown in Figure 6, along with the labeling used in that plot, for comparison.

data, with similar counts to other regions, but clearly has a much wider range of intensities associated with it when compared against other regions in Figure 6b. Less can be ascertained from the midnight sector of the map, where almost no data exists. A bright enhancement occurs at the dawn edge of this missing region, but might relate to lower count rates in this region.

#### 2.4.1. Individual Planetary Local Time Images Mapped Into Magnetic Coordinates

Figure 7 shows each individual local time magnetic map, in order to try and better constrain the average map shown in Figure 6. For clarity, since the data is sparser within individual images than when all five images are combined, we instead bin the data into  $10 \times 10 R_I$  gridding.

The only consistent feature observed across all five planetary local time sectors is the broad region of significantly enhanced emission at dusk, with this region typically strongest closer to the planet and fading by approximately a half at the region close to the magnetopause boundary. Noonward of this bright dusk feature, there is a consistent darkening in the auroral emission. This is approximately co-located with the  $\Delta I$  region, but the darkening appears to sweep across this region with changing local time: at 08hr the darkening is westward of the  $\Delta I$  region, and yet by 16hr, the darkest region is eastwards of this region. This might potentially be an offset in the mapping produced by the Vogt et al. (2011) model, might indicate a shift in the location of aurorally-associated processes as the auroral region swings from dawn facing to dusk facing, or might just be the results of enhanced errors close to the planetary limb.

Both 08 and 16 hr show strong enhancement on both dawn and dusk sides of the magnetosphere, which could be a real effect, or the result of fringes of enhancement close to the edge of the planet impacting the data. It may, for instance, be associated with the strong dusk enhancement seen in both auroral and equatorial emission observed in Paper 1. It suggests we are pushing the image data about as far as we are able, and so while these maps are broadly instructive, we must be careful to not read too far into their small-scale details.

#### 2.4.2. Comparisons With Rutala et al. (2024)

As discussed within the introduction, a comprehensive comparison between this data set and the UV mapped emissions shown in Rutala et al. (2024) is challenging, since that paper does not account for either the changing surface magnetic field or planetary local time. Past measurements have suggested magnetic field strength at Jupiter is strongly anti-correlated with the statistical UV brightness, at least in comparing the brightness of each hemisphere (Bonfond et al., 2015). Theoretically, the brightness changes observed in the H<sub>3</sub><sup>+</sup> brightness are likely to also drive comparable changes in UV brightness, as described in Paper 1. Figure 2 of Rutala et al. (2024) provides a multi-panel plot of UV brightness with local time and distance for a range of planetary longitudes in both the north and south, against which we can compare our measurements.

In Figure 8, we plot our data set into magnetic local time and distance from the planet, a comparable set of axes to those shown in Figure 2 of Rutala et al. (2024), using a 1 hr  $\times$  10 R<sub>J</sub> gridding. This data is shown over two ranges, our entire data set between 0 and 150 R<sub>J</sub> and the narrower range of distances shown in Figure 2 of Rutala

STALLARD ET AL. 18 of 24

from https://agupubs.onlinelibrary.wiley.com/doi/10.1029/2025JA034076 by NICE, National Institute for Health and Care Excellence, Wiley Online Library on [16/10/2025]. See the Terms

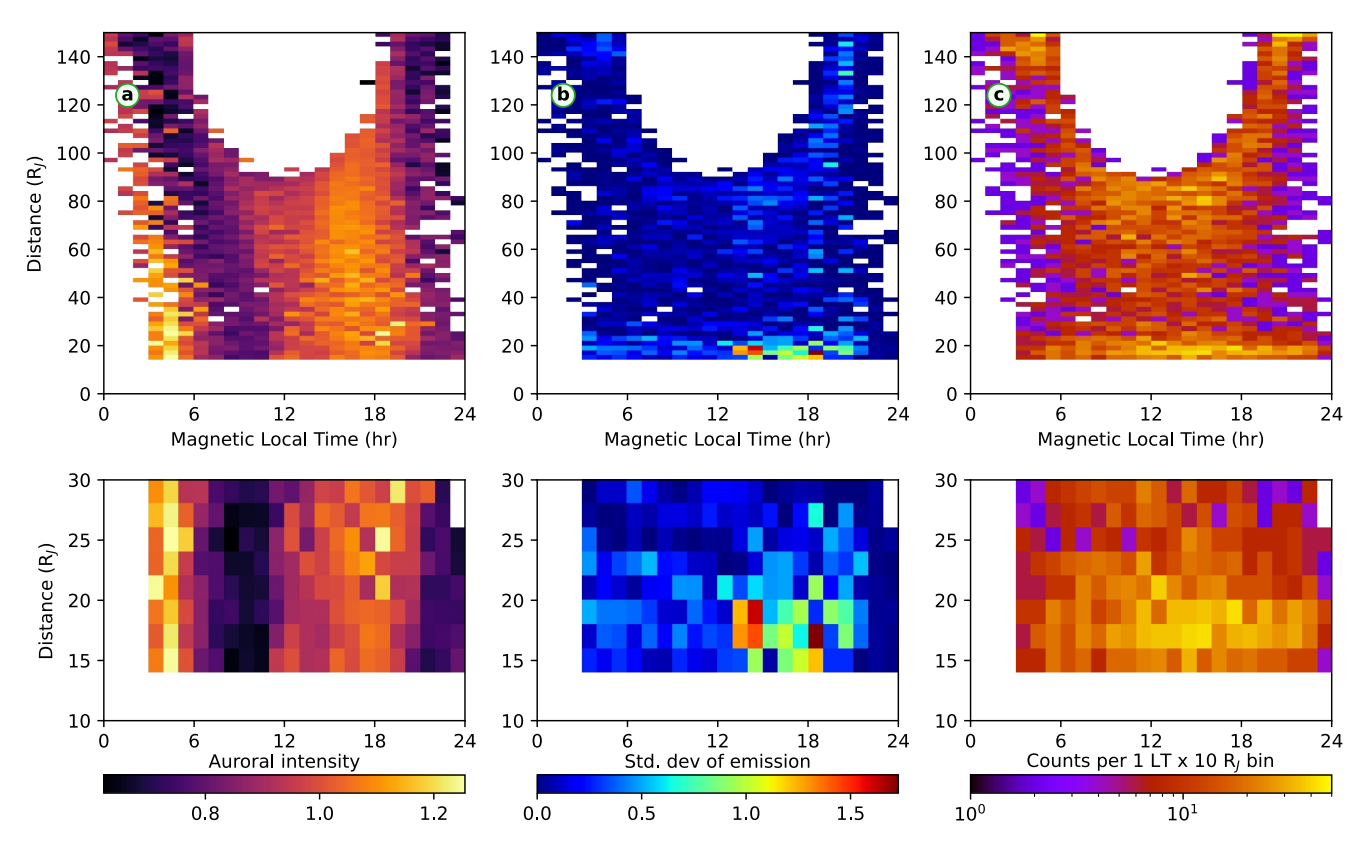


**Figure 8.** Magnetically mapped auroral emission brightness, standard deviation and count numbers. The top three panels show the local time and radial distance in Jovian radii within Jupiter's magnetosphere. The left panel (a) shows the mean auroral emission from the five sectors mapped into magnetospheric coordinates. Different regions see significant variation in the standard deviation of the pixel brightness mapped into that region, shown in the central panel (b), with total numbers of pixels taken from the five images shown in Figure 5 is shown on the right (c). The bottom panels shows the same emission, but over the distance scale used in Figure 2 of Rutala et al. (2024).

et al. (2024), between 10 and  $30\,R_J$ . Here, our data includes corrections for both planetary local time and magnetic field strength, as above. Removing this correction in our data set seems to enhance emission pre-noon, and reduce emission post-noon, as shown in the Supporting Information S1, but the affects on Rutala et al. (2024)'s data may differ, depending upon what the biases in Jupiter's rotational phase are within the observational data set used there.

There are no clear comparable features within the northern auroral maps presented in Rutala et al. (2024) and Figure 8, suggesting either the affect of varying magnetic field strength and/or planetary local time are distorting Rutala et al. (2024)'s view of the emission, that the UV data set represents a different overall average (perhaps because one or both data sets fails to take into account the wide range of jovian auroral variation), or because Jupiter's northern UV emission is fundamentally different in emission structure to the northern  $H_3^+$  emission.

However, it is perhaps notable that the southern auroral emission structures observed at some longitudes in Rutala et al. (2024) do appear to align much more closely with the data as it is mapped here. At longitudes between 288 and 360 solar CML, Rutala et al. (2024) shows significant darkening at local times between 6 and 12 UT, matching with the darkening observed in Figure 8. At 24–48 solar CML, Rutala et al. (2024) shows a strong enhancement observed at ~6 UT, again aligning with our observed structure. While potentially co-incidental, it is notable that these comparable brightness changes do seem to occur in the hemisphere with the smallest changes in magnetic field strength, perhaps implying that Rutala et al. (2024)'s northern observations are strongly affected by magnetic field differences (though this does not explain why that data set observes brighter emission in the north than the south).

We also note that the middle panel of Figure 8 clearly reveals a strong dusk enhancement in variability. This highlights that the duskward main emission is more strongly variable in absolute terms than any other region of Jupiter's aurora, a statistical bias perhaps associated with the incredibly bright short-lived dusk enhancements

STALLARD ET AL. 19 of 24

recently observed with JWST (J. D. Nichols et al., 2025), produced by enhanced  $H_3^+$  ionization, but strangely without any UV emission enhancement.

#### 3. Discussion

Jupiter's auroral emission is highly variable and complex, even with the prodigious amount of data used in this study. After splitting the data into five local time sectors then mapping these sectors into both polar regions and magnetospheric local time and planetary distance, we are close to the limit of our ability to discern statistically significant influences on the auroral structures seen at Jupiter.

As noted in Paper 1, this study is of only limited utility in understanding the underlying drivers of brightness differences within the UV H and  $\rm H_2$  emission, with significant variation caused by differences in the altitude of the precipitating particles that cause these two sources of auroral emission. However, on the main auroral emission at least, UV emission is likely also strongly modulated by both planetary local time and magnetic field strength.

Equally, the strong variations in main auroral emission strength with magnetically mapped location are also likely to see parallels with the UV emission brightness, with the strong enhancement in dusk side emission having been tentatively identified by Bonfond et al. (2015) (tentative only because magnetic field could not be fully accounted for in that study), and the dawn to noon dimming observed in the southern auroral region, at least at some longitudes, observed by Rutala et al. (2024).

However, while these arguments hold to some degree within the main auroral emission and, perhaps, the Active and Dark polar regions, they break down completely within the Swirl region, because this region has very high color ratio UV emission that appears to be driven from very high precipitating energy particles deep in the ionosphere, well beneath the homopause, and yet are also often strongly associated with bright  $H_3^+$  emissions. This apparent contradiction might originate from an inflated homopause driven by auroral heating over the magnetic pole (Sinclair et al., 2020). Alternatively, the detection of very high energy (>10 MeV) precipitation by Juno within the Swirl region (Paranicas et al., 2018) might instead indicate two different particle flux energy populations, one very high energy, producing deep UV emissions and the other relatively low energy (Tao et al., 2011 predict that  $H_3^+$  eeission dominates by orders of magnitude at very low energy, and start to dominate at particle energies <10 keV). Either way, this unresolved issue makes it difficult to argue about how UV and  $H_3^+$  might compare.

This investigation has revealed several very strong controls on the northern  $H_3^+$  emission brightness within the magnetically mapped source regions:

- 1. There is a clear enhancement of emission in regions mapping to magnetospheric dusk, even when accounting for the different mapping size on the planet. This directly agrees with Bonfond et al. (2015) who identified this asymmetry in UV observations at a much more constrained range of planetary local times. As stated in that paper, this would be difficult to produce through a current system closing through the planet, as you might expect an approximate balance in emission on dawn and dusk from asymmetric plasma flow within the magnetosphere (as at Earth), as well as the obvious balance from axisymmetric breakdown in corotation currents.
  - Since Paper 1 clearly identified a strong planetary local time enhancement along the main auroral emission, the auroral brightness across all planetary local times is directly linked to currents flowing between the magnetosphere and ionosphere, in agreement with J. D. Nichols and Cowley (2022)'s correlation measured near dawn. However, with only ~7% of precipitation resulting from discrete acceleration (Salveter et al., 2022; measuring mostly in Region-A, and across unstated local times), these currents cannot themselves drive the aurora, perhaps instead triggering cascades of increasing instability in the magnetosphere.
  - However, perhaps instabilities can be controlled by more than just the breakdown-in-corotation currents, despite the linear relationship suggested at noon by (J. D. Nichols & Cowley, 2022). If downward currents drove similar levels of instability, they could produce equivalent broadband infall, lacking only the small ~7% of precipitation resulting from discrete acceleration of electrons.
  - This would allow broad regions dominated by upward electrons (downward currents; Zone II aurora) to be
    directly controlled by the changing ionospheric conditions, even if those currents closing within such

STALLARD ET AL. 20 of 24

regions cannot produce accelerated discrete precipitation. It might also help explain the sharp contrast in apparent precipitation energy between the main aurora and poleward Zone II emission (as highlighted by low UV color ratio and relatively strong  $H_3^+$  emission).

- 2. There is some evidence that the weakening of the main emission in the pre-noon region (as observed by Radioti et al., 2008), previously attributed to asymmetric magnetospheric flows diminishing this specific region (Chané et al., 2013), appears to move in magnetospheric local time with changing planetary local time.
  - This suggests either that the dynamics associated with this weakening are warped by the wobble induced by
    magnetic field lines rotating around the Jovigraphic pole, or that the mapping from the Vogt et al. (2011)
    model does not capture the complex stretching and warping of field lines in this region.
- 3. The H<sub>3</sub><sup>+</sup> polar emission changes dramatically in the auroral morphology with changing planetary local time. This strongly suggests that either the processes that drive precipitation into the polar region undergo significant changes as the polar magnetic field lines move around the rotational pole, or that the magnetic mapping from the ionosphere out into regions of the magnetosphere or surrounding solar wind undergo significant changes as the planet rotates.
  - (a) Comparisons between the H<sub>3</sub><sup>+</sup> polar emission morphology and the statistically averaged polar regions calculated within the axisymmetric Zhang et al. (2021) model reveal similarities when the polar region points dawnward.
  - (b) The Dark region rotates around the auroral region, always found approximately on the Dawn side of the polar auroral region. This strongly suggests this is a relative fixed feature, seen in on the solar dawnward side no matter the rotational phase of the planet. This confirms the findings of the Juno UVS, which measured this region at magnetic local times of between 0 and 11 UT (Greathouse et al., 2021).
    - This region was recently identified by Delamere et al. (2024) as strongly associated with magnetic field lines open to the solar wind. Notably, JEDI integral moments showed that the He<sup>n+</sup>/H<sup>+</sup> ratio in this region is consistent with open field lines and solar wind composition.
    - In addition, JADE numerical moments showed, on average, anti-corotational flow within that same region, directly aligning this 'open' region with the strongly sub-corotating Dark region observed in ground-based ion velocity measurements (Johnson et al., 2017).
    - Our observations clearly show this region is fixed in local time and strengthens the argument in Delamere et al. (2024) that the Dark region is the open-field-line region in Jupiter's polar aurora.
    - This region does appear to move slightly faster than the planet, suggesting it is drifting toward midnight
      as the magnetic pole moves into dusk, perhaps indicating the field lines map differently with changing
      magnetic pole direction.
  - (c) The Swirl region, however, changes in its morphology significantly as it rotates around toward dusk, no longer aligns with the regions described in Zhang et al. (2021).
    - Given that the regions detailed in Zhang et al. (2021) were highly sporadic on shorter timescales and were only clearly revealed once the model was run for four full days, the specific location of open flux is clearly highly dependent upon the instantaneous MHD coupling.
    - While this region has been observed to significantly sub-corotate (Johnson et al., 2017; Stallard et al., 2001), when compared with the coinciding neutral atmosphere, they appear to slightly blue-shift toward the Sun (R. Wang et al., 2023). This might indicate a magnetospheric flow, or that this region is dominated by neutrals forcing ions into sub-corotation with the planet's auroral vortex.
    - However, all ionospheric velocity observations so far have been made when region has been on the
      dawn side of the planet. Future ion and neutral wind measurements across a wide range of longitudes
      are essential to better understand the influence of planetary local time on the Swirl region.
    - If this is a result of the changing conditions in the dawnside magnetosphere with changing magnetic
      pole direction, a re-analysis of the dawnside measurements of Juno with changing CML could resolve
      the cause of this change.
    - However, if this originates from changing mapping, only detailed ionospheric measurements and/or
      magnetospheric modeling using a tilted higher-order magnetic field model will help in explaining these
      shift in emission.

#### 4. Conclusion

This study provides a unique window past the breath-taking complexity observed in Jupiter's aurora, giving us the first unrestricted views of the underlying magnetospheric structures that drive this emission.

STALLARD ET AL. 21 of 24

Acknowledgments

T.S.S. and E.M.T. were supported by the

STFC Consolidated Grant (ST/W00089X/

1). H.M. was supported by the STFC James

Webb Fellowship (ST/W001527/2). L.M.

was supported by Grant 80NSSC20K1045

Workings program. J.O'D. was supported

by the STFC Ernest Rutherford Fellowship

(ST/X003426/1). K.L.K. was supported by

Studentship. J.C.C. was supported by the

(ST/V004883/1). Data were provided by

the Magnetospheres of the Outer Planets

maintained by Makenzie Lystrup. J.E.P.

Telescope Facility, which is operated by

08AE38A with the National Aeronautics

Mission Directorate, Planetary Astronomy

Program. This research was supported by

the International Space Science Institute

(ISSI) in Bern, through ISSI International

Connerney and Takehiko Satoh were visiting astronomers at the NASA Infrared

Infrared Data Archive, Laboratory for

Atmospheric and Space Physics,

University of Colorado Boulder,

the University of Hawaii under

Cooperative Agreement no. NNX-

and Space Administration, Science

Team project #592.

a Northumbria University Research

STFC Ernest Rutherford Fellowship

issued through the NASA Solar System

It reveals a main emission that is directly shaped by the magnetic mapping from the planet's surface out into the surrounding magnetosphere, a mapping that is in turn strongly modulated by planetary local time. It also reveals a clear asymmetry in the emission between dawn and dusk, and a local minimum near noon, features long suggested in past observations, but often lost in the array of varying aurora observed on an individual day.

It also provides direct information about the enigmatic emission in the pole, with past models of the polar regions correlating to the observed morphology under some local times, but that this interaction clearly changes dramatically with local time and is far more complex than current models predict.

Ultimately, however, the data set used here is also limited in its ability to reveal detail. Ground-based measurements are limited in their spatial accuracy, and can only provide a view of the auroral region across less than half of all local times. Fortunately, the Juno mission's observations of Jupiter's aurora at incredible spatial scales and a wide range of local times likely mean there are enough images to provide clear statistical averages for changing latitude, longitude, local time and potentially even for changing magnetospheric driving (e.g., from changing solar wind conditions). As a result, maps of varying auroral emission brightness and UV spectral color at much higher levels of detail will become viable. These promise to reveal far more than this preliminary study was able to, and may represent a profound shift in our understanding of auroral processes at Jupiter.

#### **Inclusion in Global Research Statement**

A clear understanding was reached among collaborators with regard to their roles, responsibilities and conduct throughout the research cycle, from study design through to study implementation, review and dissemination.

#### **Data Availability Statement**

Data and code to produce the figures in this paper are available from Stallard (2025).

#### References

Bonfond, B., Grodent, D., Gérard, J. C., Stallard, T. S., Clarke, J. T., Yoneda, M., et al. (2012). Auroral evidence of Io's control over the magnetosphere of Jupiter. Geophysical Research Letters, 39(1), L01105. https://doi.org/10.1029/2011GL050253

Bonfond, B., Gustin, J., Gérard, J. C., Grodent, D., Radioti, A., Palmaerts, B., et al. (2015). The far-ultraviolet main auroral emission at Jupiter–Part I: Dawn-dusk brightness asymmetries. *Annales Geophysicae*, 33(10), 1203–1209. https://doi.org/10.5194/angeo-33-1203-2015

Bonfond, B., Saur, J., Grodent, D., Badman, S. V., Bisikalo, D., Shematovich, V., et al. (2017). The tails of the satellite auroral footprints at Jupiter. Journal of Geophysical Research (Space Physics), 122(8), 7985–7996. https://doi.org/10.1002/2017JA024370

Caldwell, J., Turgeon, B., & Hua, X. M. (1992). Hubble space telescope imaging of the north polar Aurora on Jupiter. *Science*, 257(5076), 1512–1515. https://doi.org/10.1126/science.257.5076.1512

Chané, E., Saur, J., & Poedts, S. (2013). Modeling Jupiter's magnetosphere: Influence of the internal sources. *Journal of Geophysical Research* (Space Physics), 118(5), 2157–2172. https://doi.org/10.1002/jgra.50258

Connerney, J. E. P., Acuña, M. H., Ness, N. F., & Satoh, T. (1998). New models of Jupiter's magnetic field constrained by the Io flux tube footprint. *Journal of Geophysical Research*, 103(A6), 11929–11940. https://doi.org/10.1029/97JA03726

Connerney, J. E. P., Baron, R., Satoh, T., & Owen, T. (1993). Images of excited H\_3+ at the foot of the Io flux tube in Jupiter's atmosphere. Science, 262(5136), 1035–1038. https://doi.org/10.1126/science.262.5136.1035

Connerney, J. E. P., Kotsiaros, S., Oliversen, R. J., Espley, J. R., Joergensen, J. L., Joergensen, P. S., et al. (2018). A new model of Jupiter's magnetic field from Juno's first nine orbits. *Geophysical Research Letters*, 45(6), 2590–2596. https://doi.org/10.1002/2018GL077312

Connerney, J. E. P., Timmins, S., Oliversen, R. J., Espley, J. R., Joergensen, J. L., Kotsiaros, S., et al. (2022). A new model of Jupiter's magnetic field at the completion of Juno's prime Mission. *Journal of Geophysical Research (Planets)*, 127(2), e07055. https://doi.org/10.1029/2021JE007055

Cowley, S. W. H., Bunce, E. J., Stallard, T. S., & Miller, S. (2003). Jupiter's polar ionospheric flows: Theoretical interpretation. *Geophysical Research Letters*, 30(5), 1220. https://doi.org/10.1029/2002GL016030

Delamere, P. A., & Bagenal, F. (2013). Magnetotail structure of the giant magnetospheres: Implications of the viscous interaction with the solar wind. *Journal of Geophysical Research (Space Physics)*, 118(11), 7045–7053. https://doi.org/10.1002/2013JA019179

Delamere, P. A., Wilson, R. J., Wing, S., Smith, A. R., Mino, B., Spitler, C., et al. (2024). Signatures of open magnetic flux in Jupiter's dawnside magnetotail. AGU Advances, 5(2), e2023AV001111. https://doi.org/10.1029/2023AV001111

Dunn, W. R., Gray, R., Wibisono, A. D., Lamy, L., Louis, C., Badman, S. V., et al. (2020). Comparisons between Jupiter's X-ray, UV and radio emissions and In-Situ solar wind measurements during 2007. *Journal of Geophysical Research (Space Physics)*, 125(6), e27222. https://doi.org/10.1029/2019JA027222

Fletcher, L., Dennis, B. R., Hudson, H. S., Krucker, S., Phillips, K., Veronig, A., et al. (2011). An observational overview of solar flares. Space Science Reviews, 159(1–4), 19–106. https://doi.org/10.1007/s11214-010-9701-8

Gerard, J.-C., Dols, V., Paresce, F., & Prange, R. (1993). Morphology and time variation of the Jovian far UV aurora: Hubble Space Telescope observations. *Journal of Geophysical Research*, 98(E10), 18793–18802. https://doi.org/10.1029/93JE01334

Gérard, J. C., Grodent, D., Radioti, A., Bonfond, B., & Clarke, J. T. (2013). Hubble observations of Jupiter's north-south conjugate ultraviolet Aurora. Icarus, 226(2), 1559–1567. https://doi.org/10.1016/j.icarus.2013.08.017

Gérard, J. C., Gustin, J., Grodent, D., Clarke, J. T., & Grard, A. (2003). Spectral observations of transient features in the FUV Jovian polar Aurora. Journal of Geophysical Research (Space Physics), 108(A8), 1319. https://doi.org/10.1029/2003JA009901

STALLARD ET AL. 22 of 24

- Gérard, J. C., Mura, A., Bonfond, B., Gladstone, G. R., Adriani, A., Hue, V., et al. (2018). Concurrent ultraviolet and infrared observations of the north Jovian Aurora during Juno's first perijove. *Icarus*, 312, 145–156. https://doi.org/10.1016/j.icarus.2018.04.020
- Gray, R. L., Badman, S. V., Woodfield, E. E., & Tao, C. (2017). Characterization of Jupiter's secondary auroral oval and its response to hot plasma injections. *Journal of Geophysical Research (Space Physics)*, 122(6), 6415–6429. https://doi.org/10.1002/2017JA024214
- Greathouse, T., Gladstone, R., Versteeg, M., Hue, V., Kammer, J., Giles, R., et al. (2021). Local time dependence of Jupiter's polar auroral emissions observed by Juno UVS. *Journal of Geophysical Research (Planets)*, 126(12), e06954. https://doi.org/10.1029/2021JE006954
- Grodent, D. (2015). A brief review of ultraviolet auroral emissions on giant planets. Space Science Reviews, 187(1-4), 23-50. https://doi.org/10.1007/s11214-014-0052-8
- Grodent, D., & Bonfond, B. (2014). Jupiter's polar auroral dynamics. Aas/division for planetary sciences meeting abstracts, 46, 422.02.
- Grodent, D., Bonfond, B., GéRard, J.-C., Radioti, A., Gustin, J., Clarke, J. T., et al. (2008). Auroral evidence of a localized magnetic anomaly in Jupiter's northern hemisphere. *Journal of Geophysical Research (Space Physics)*, 113(A9), A09201. https://doi.org/10.1029/2008JA013185
- Grodent, D., Clarke, J. T., Kim, J., Waite, J. H., & Cowley, S. W. H. (2003a). Jupiter's main auroral oval observed with HST-STIS. Journal of Geophysical Research (Space Physics), 108(A11), 1389. https://doi.org/10.1029/2003JA009921
- Grodent, D., Clarke, J. T., Waite, J. H., Cowley, S. W. H., GéRard, J. C., & Kim, J. (2003b). Jupiter's polar auroral emissions. *Journal of Geophysical Research (Space Physics)*, 108(A10), 1366. https://doi.org/10.1029/2003JA010017
- Gustin, J., Grodent, D., Ray, L. C., Bonfond, B., Bunce, E. J., Nichols, J. D., & Ozak, N. (2016). Characteristics of north Jovian aurora from STIS FUV spectral images. *Icarus*, 268, 215–241. https://doi.org/10.1016/j.icarus.2015.12.048
- Haewsantati, K., Bonfond, B., Wannawichian, S., Gladstone, G. R., Hue, V., Greathouse, T. K., et al. (2023). Juno's multi-instruments observations during the flybys of auroral bright spots in Jupiter's polar aurorae. *Journal of Geophysical Research (Space Physics)*, 128(8), e2023JA031396. https://doi.org/10.1029/2023JA031396
- Hill, T. W. (1979). Inertial limit on corotation. *Journal of Geophysics Research*, 84(A11), 6554–6558. https://doi.org/10.1029/JA084iA11p06554
  Hue, V., Gladstone, G. R., Louis, C. K., Greathouse, T. K., Bonfond, B., Szalay, J. R., et al. (2023). The Io, europa, and ganymede auroral footprints at Jupiter in the ultraviolet: Positions and equatorial lead angles. *Journal of Geophysical Research (Space Physics)*, 128(5), e2023JA031363. https://doi.org/10.1029/2023JA031363
- Johnson, R. E., Melin, H., Stallard, T. S., Tao, C., Nichols, J. D., & Chowdhury, M. N. (2018). Mapping H<sub>3</sub><sup>+</sup> temperatures in Jupiter's Northern auroral ionosphere using VLT-CRIRES. *Journal of Geophysical Research (Space Physics)*, 123(7), 5990–6008. https://doi.org/10.1029/2018JA025511
- Johnson, R. E., Stallard, T. S., Melin, H., Nichols, J. D., & Cowley, S. W. H. (2017). Jupiter's polar ionospheric flows: High resolution mapping of spectral intensity and line-of-sight velocity of H<sub>3</sub><sup>+</sup> ions. *Journal of Geophysical Research (Space Physics)*, 122(7), 7599–7618. https://doi.org/10.1002/2017JA024176
- Kivelson, M. G., & Southwood, D. J. (2005). Dynamical consequences of two modes of centrifugal instability in Jupiter's outer magnetosphere. Journal of Geophysical Research (Space Physics), 110(A12), A12209. https://doi.org/10.1029/2005JA011176
- Kotsiaros, S., Connerney, J. E. P., Clark, G., Allegrini, F., Gladstone, G. R., Kurth, W. S., et al. (2019). Birkeland currents in Jupiter's magnetosphere observed by the polar-orbiting Juno spacecraft. *Nature Astronomy*, 3(10), 904–909. https://doi.org/10.1038/s41550-019-0819-7
- Krupp, N., Lagg, A., Livi, S., Wilken, B., Woch, J., Roelof, E. C., & Williams, D. J. (2001). Global flows of energetic ions in Jupiter's equatorial plane: First-order approximation. *Journal of Geophysics Research*, 106(A11), 26017–26032. https://doi.org/10.1029/2000JA900138
- Masters, A., Dunn, W. R., Stallard, T. S., Manners, H., & Stawarz, J. (2021). Magnetic reconnection near the planet as a possible driver of Jupiter's mysterious polar auroras. *Journal of Geophysical Research (Space Physics)*, 126(8), e29544. https://doi.org/10.1029/2021JA029544
- Mauk, B. H., Clark, G., Gladstone, G. R., Kotsiaros, S., Adriani, A., Allegrini, F., et al. (2020). Energetic particles and acceleration regions over Jupiter's polar cap and main Aurora: A broad overview. *Journal of Geophysical Research (Space Physics)*, 125(3), e27699. https://doi.org/10. 1029/20191A027699
- Mauk, B. H., Haggerty, D. K., Paranicas, C., Clark, G., Kollmann, P., Rymer, A. M., et al. (2017). Discrete and broadband electron acceleration in Jupiter's powerful Aurora. *Nature*, 549(7670), 66–69. https://doi.org/10.1038/nature23648
- Mauk, B. H., Ma, Q., Becker, H. N., Jørgensen, J. L., Denver, T., Connerney, J. E. P., et al. (2024). Upward, MeV-Class electron beams over Jupiter's main Aurora. Geophysical Research Letters, 51(24), 2024GL108799. https://doi.org/10.1029/2024GL108799
- Milan, S. E., Bunce, E. J., Cowley, S. W. H., & Jackman, C. M. (2005). Implications of rapid planetary rotation for the dungey magnetotail of Saturn. *Journal of Geophysical Research (Space Physics)*, 110(A3), A03209. https://doi.org/10.1029/2004JA010716
- Moore, L., O'Donoghue, J., Melin, H., Stallard, T. S., Tao, C., Zieger, B., et al. (2017). Variability of Jupiter's IR H<sub>3</sub><sup>+</sup> aurorae during Juno approach. *Geophysical Research Letters*, 44(10), 4513–4522. https://doi.org/10.1002/2017GL073156
- Mura, A., Adriani, A., Altieri, F., Connerney, J. E. P., Bolton, S. J., Moriconi, M. L., et al. (2017). Infrared observations of Jovian aurora from Juno's first orbits: Main oval and satellite footprints. *Geophysics Research Letters*, 44(11), 5308–5316. https://doi.org/10.1002/2017GL072954
- Mura, A., Adriani, A., Connerney, J. E. P., Bolton, S., Altieri, F., Bagenal, F., et al. (2018). Juno observations of spot structures and a split tail in Io-induced aurorae on Jupiter. *Science*, 361(6404), 774–777. https://doi.org/10.1126/science.aat1450
- Mura, A., Moirano, A., Hue, V., Castagnoli, C., Migliorini, A., Altieri, F., et al. (2025). Vertical and temporal H<sub>3</sub><sup>+</sup> structure at the auroral footprint of Io. *The Planetary Science Journal*, 6(2), 49. https://doi.org/10.3847/PSJ/ada6aa
- Nichols, J., & Cowley, S. (2004). Magnetosphere-ionosphere coupling currents in Jupiter's middle magnetosphere: Effect of precipitation-induced enhancement of the ionospheric Pedersen conductivity. *Annales Geophysicae*, 22(5), 1799–1827. https://doi.org/10.5194/angeo-22-1799-2004
- Nichols, J. D., & Cowley, S. W. H. (2022). Relation of jupiter's dawnside main emission intensity to magnetospheric currents during the juno mission. *Journal of Geophysical Research (Space Physics)*, 127(1), e30040. https://doi.org/10.1029/2021JA030040
- Nichols, J. D., King, O. R. T., Clarke, J. T., de Pater, I., Fletcher, L. N., Melin, H., et al. (2025). Dynamic infrared Aurora on Jupiter. Nature Communications, 16(1), 3907. https://doi.org/10.1038/s41467-025-58984-z
- Pallier, L., & Prangé, R. (2001). More about the structure of the high latitude Jovian aurorae. *Planetary and Space Science*, 49(10–11), 1159–1173. https://doi.org/10.1016/S0032-0633(01)00023-X
- Paranicas, C., Mauk, B. H., Haggerty, D. K., Clark, G., Kollmann, P., Rymer, A. M., et al. (2018). Intervals of intense energetic electron beams over Jupiter's poles. *Journal of Geophysical Research (Space Physics)*, 123(3), 1989–1999. https://doi.org/10.1002/2017JA025106
- Radioti, A., GéRard, J. C., Grodent, D., Bonfond, B., Krupp, N., & Woch, J. (2008). Discontinuity in Jupiter's main auroral oval. *Journal of Geophysical Research (Space Physics)*, 113(A1), A01215. https://doi.org/10.1029/2007JA012610
- Radioti, A., Tomás, A. T., Grodent, D., Gérard, J. C., Gustin, J., Bonford, B., et al. (2009). Equatorward diffuse auroral emissions at Jupiter: Simultaneous HST and Galileo observations. *Geophysical Research Letters*, 36(7), L07101. https://doi.org/10.1029/2009GL037857
- Ray, L. C., Achilleos, N. A., Vogt, M. F., & Yates, J. N. (2014). Local time variations in Jupiter's magnetosphere-ionosphere coupling system. Journal of Geophysical Research (Space Physics), 119(6), 4740–4751. https://doi.org/10.1002/2014JA019941

STALLARD ET AL. 23 of 24

- Rutala, M. J., Clarke, J. T., Vogt, M. F., & Nichols, J. D. (2024). Variation in the pedersen conductance near Jupiter's main emission Aurora: Comparison of hubble space telescope and galileo measurements. *Journal of Geophysical Research (Space Physics)*, 129(3), e2023JA032122. https://doi.org/10.1029/2023JA032122
- Salveter, A., Saur, J., Clark, G., & Mauk, B. H. (2022). Jovian auroral electron precipitation budget—A statistical analysis of diffuse, monoenergetic, and broadband auroral electron distributions. *Journal of Geophysical Research (Space Physics)*, 127(8), e30224. https://doi.org/10.1029/20214030224
- Satoh, T., & Connerney, J. E. P. (1999). Jupiter's H<sub>3</sub><sup>+</sup> emissions viewed in corrected jovimagnetic coordinates. *Icarus*, 141(2), 236–252. https://doi.org/10.1006/icar.1999.6173
- Shure, M., Toomey, D. W., Rayner, J., Onaka, P., Denault, A., Stahlberger, W., et al. (1994). A powerful new infrared Array camera for the Nasa Infrared telescope facility. I. S. McLean (Ed.), In Astronomy with arrays, the next generation (Vol. 190, pp. 395–398). https://doi.org/10.1007/978-94-011-1070-9 126
- Sinclair, J. A., Greathouse, T. K., Giles, R. S., Antuñano, A., Moses, J. I., Fouchet, T., et al. (2020). Spatial variations in the altitude of the CH<sub>4</sub> homopause at Jupiter's mid-to-high latitudes, as constrained from IRTF-TEXES spectra. *Planetary Science Journal*, 1(3), 85. https://doi.org/10.3847/PSJ/abc887
- Stallard, T. (2025). Jupiter's varying auroral emission 2: Plot data and code [collection]. Harvard Dataverse. https://doi.org/10.7910/DVN/VOVEF1
- Stallard, T. S. (2018). The magnetospheres of the outer planets infrared data archive: IRTF NSFCAM 1995–2000. Harvard Dataverse. https://doi.org/10.7910/DVN/K/VOWNI
- Stallard, T. S., Burrell, A. G., Melin, H., Fletcher, L. N., Miller, S., Moore, L., et al. (2018). Identification of Jupiter's magnetic equator through H<sub>3</sub><sup>+</sup> ionospheric emission. *Nature Astronomy*, 2(10), 773–777. https://doi.org/10.1038/s41550-018-0523-z
- Stallard, T. S., Clarke, J. T., Melin, H., Miller, S., Nichols, J. D., O'Donoghue, J., et al. (2016). Stability within Jupiter's polar auroral "Swirl region" over moderate timescales. *Icarus*, 268, 145–155. https://doi.org/10.1016/j.icarus.2015.12.044
- Stallard, T. S., Miller, S., Millward, G., & Joseph, R. D. (2001). On the dynamics of the jovian ionosphere and thermosphere. I. The measurement of ion winds. *Icarus*, 154(2), 475-491. https://doi.org/10.1006/icar.2001.6681
- Sulaiman, A. H., Mauk, B. H., Szalay, J. R., Allegrini, F., Clark, G., Gladstone, G. R., et al. (2022). Jupiter's low-altitude auroral zones: Fields, particles, plasma waves, and density depletions. *Journal of Geophysical Research (Space Physics)*, 127(8), e30334. https://doi.org/10.1029/2022JA030334
- Tao, C., Badman, S. V., & Fujimoto, M. (2011). UV and IR auroral emission model for the outer planets: Jupiter and Saturn comparison. *Icarus*, 213(2), 581–592. https://doi.org/10.1016/j.icarus.2011.04.001
- Tao, C., Fujiwara, H., & Kasaba, Y. (2010). Jovian magnetosphere-ionosphere current system characterized by diurnal variation of ionospheric conductance. *Planetary and Space Science*, 58(3), 351–364. https://doi.org/10.1016/j.pss.2009.10.005
- Vogt, M. F., Bunce, E. J., Kivelson, M. G., Khurana, K. K., Walker, R. J., Radioti, A., et al. (2015). Magnetosphere-ionosphere mapping at Jupiter: Quantifying the effects of using different internal field models. *Journal of Geophysical Research (Space Physics)*, 120(4), 2584–2599. https://doi.org/10.1002/2014JA020729
- Vogt, M. F., Kivelson, M. G., Khurana, K. K., Walker, R. J., Bonfond, B., Grodent, D., & Radioti, A. (2011). Improved mapping of Jupiter's auroral features to magnetospheric sources. *Journal of Geophysical Research (Space Physics)*, 116(A3), A03220. https://doi.org/10.1029/ 20101A016148
- Wang, J.-Z., Bagenal, F., Wilson, R. J., Nerney, E., Ebert, R. W., Valek, P. W., et al. (2024). Dawn-dusk asymmetry of plasma flow in Jupiter's Middle magnetosphere observed by Juno. *Geophysical Research Letters*, 51(19), e2024GL110209. https://doi.org/10.1029/2024GL110209
- Wang, R., Stallard, T. S., Melin, H., Baines, K. H., Achilleos, N., Rymer, A. M., et al. (2023). Asymmetric ionospheric jets in Jupiter's Aurora. Journal of Geophysical Research (Space Physics), 128(12), e2023JA031861. https://doi.org/10.1029/2023JA031861
- Zhang, B., Delamere, P. A., Yao, Z., Bonfond, B., Lin, D., Sorathia, K. A., et al. (2021). How Jupiter's unusual magnetospheric topology structures its aurora. *Science Advances*, 7(15), eabd1204. https://doi.org/10.1126/sciadv.abd1204

STALLARD ET AL. 24 of 24